
DeMa: Dual-Path Delay-Aware Mamba for Efficient Multivariate Time Series Analysis

Rui An^{1,2,*}, Haohao Qu^{2,*}, Wenqi Fan², Xuequn Shang¹, Qing Li²

¹Northwestern Polytechnical University, ²The Hong Kong Polytechnic University
 {rui77.an, haohao.qu}@connect.polyu.hk,
 wenqifan03@gmail.com, shang@nwpu.edu.cn, csqli@comp.polyu.edu.hk

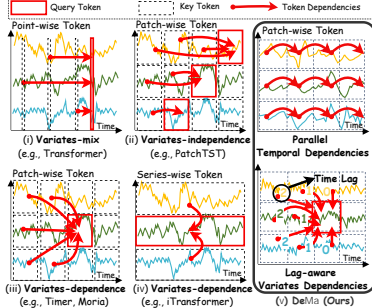
Abstract

Accurate and efficient multivariate time series (MTS) analysis is increasingly critical for a wide range of intelligent applications, including traffic forecasting, anomaly detection for industrial maintenance, and trajectory classification for health monitoring. Within this realm, Transformers have emerged as the predominant architecture due to their strong ability to capture pairwise dependencies. However, Transformer-based models suffer from quadratic computational complexity and high memory overhead, limiting their scalability and practical deployment in long-term and large-scale MTS modeling. Recently, Mamba has emerged as a promising linear-time alternative with high expressiveness. Nevertheless, directly applying vanilla Mamba to MTS remains suboptimal due to three key limitations: (i) the lack of explicit cross-variate modeling, (ii) difficulty in disentangling the entangled intra-series temporal dynamics and inter-series interactions, and (iii) insufficient modeling of latent time-lag interaction effects. These issues constrain its effectiveness across diverse MTS tasks. To address these challenges, we propose **DeMa**, a dual-path **D**elay-**A**ware **M**amba backbone for efficient and effective MTS analysis. DeMa preserves Mamba’s linear-complexity advantage while substantially improving its suitability for multivariate settings. Specifically, DeMa introduces three key innovations: (i) it decomposes the MTS context into intra-series temporal dynamics and inter-series interactions and learns them via two dedicated paths; (ii) it develops a temporal path with a *Mamba-SSD* module to capture long-range dynamics within each individual series, accommodating variable-length inputs and enabling series-independent, parallel computation while maintaining linear complexity; and (iii) it designs a variate path with a *Mamba-DALA* module that integrates delay-aware linear attention to model cross-variate dependencies, enhancing fine-grained, delay-sensitive dependency learning. Extensive experiments on five representative tasks, long- and short-term forecasting, data imputation, anomaly detection, and series classification, demonstrate that DeMa achieves state-of-the-art performance while delivering remarkable computational efficiency.

1 Introduction

Multivariate time series (**MTS**) are a crucial and fundamental data modality in both industrial and daily scenarios. They are collected at scale by physical and virtual sensors, which continuously record system measurements and encapsulate valuable information about the evolving dynamics of real-world systems [1]. Consequently, time series analysis serves as a cornerstone for understanding and predicting the behaviors of complex systems, enabling a wide range of intelligent applications,

*Equal Contribution



(a) Dependency modeling strategies.

Category	Representative Model	Temporal Dependencies	Variate Dependencies	Computational Complexity
(i)	Transformer [7]	✓	✗	$\mathcal{O}(T^2d)$
(ii)	PatchTST [8]	✓	✗	$\mathcal{O}(NL^2d)$
(iii)	Timer [9] Moria [10]	✓	✓	$\mathcal{O}(N^2L^2d)$ $\mathcal{O}(N^2L^2d)$
(iv)	iTransformer [11]	✓	✓	$\mathcal{O}(N^2d)$
(v)	DeMa (Ours)	✓	✓	$\mathcal{O}(2NLd^2)$

(b) Computational complexity comparison.

Figure 1: **Dependency modeling strategies and computational complexity of representative MTS architectures.** (a) Tokenization and induced dependency patterns (variate-mixing, variate-independent, variate-dependent). (b) Complexity comparison of representative models. Here, T is the lookback length, N the number of variates, L the token length, and d the embedding dimension, in typical long-horizon settings, $T > L \gg N, d$. **DeMa** decouples temporal modeling and delay-aware cross-variate interactions with linear-time complexity.

such as traffic flow forecasting for transportation scheduling [2, 3], missing data imputation for web stream processing [4, 5], anomaly detection for maintenance [4, 5], and trajectory classification for health monitoring [6].

Due to the complex and non-stationary nature of real-world systems, observed MTS often exhibit intricate and entangled patterns [12, 13]. Along the temporal axis, multiple variations, including long-term trends, seasonal cycles, and irregular fluctuations, are typically mixed and overlapped. Along the variate axis, correlated series interact through latent dependencies, where the evolution of one variable can influence, or be influenced by, others with time delays. Accordingly, a series of deep models have been proposed to capture *temporal dependencies* and *variate dependencies*. From the perspective of backbone architectures, existing methods can be broadly categorized into RNN-, CNN-, MLP-, and Transformer-based methods. Typically, RNN-based models [14, 15] leverage recurrent structures to model temporal state transitions, while CNN-based models [12, 16, 17] employ temporal convolutional networks (TCNs) to extract local variation patterns. However, both RNN- and CNN-based methods are constrained by limited effective receptive fields, which hinders their ability to capture long-term dependencies. Lightweight MLP-based models [18, 19] utilize stacked fully connected layers to model temporal patterns, where dense connections implicitly capture measurement-free relationships among time points within each variable [11]. These linear forecasters are primarily designed for forecasting tasks and are computationally efficient. Nevertheless, due to their architectural simplicity and limited representational capacity, MLP-based models suffer from an information bottleneck, making it difficult to represent long-range and complex temporal dependencies. Transformer-based models, which adopt attention mechanisms to capture pairwise dependencies with a global receptive field, have become mainstream for MTS modeling [20, 21, 22, 23, 8, 24, 11]. Specifically, these methods typically tokenize time series into point-wise tokens [20, 21, 22, 23], patch-wise tokens [8, 24], or series-wise tokens [11], and then apply attention to model temporal dependencies, variate dependencies, or both, as illustrated in Figure 1(a)(i-iv). Despite their remarkable performance, Transformer-based models face growing concerns regarding their *quadratic computational complexity* [25, 18], which results in substantial computational demands and memory overhead. Specifically, the cost of self-attention scales quadratically with the token length, as listed in Figure 1(b)(i-iv). For an MTS instance with N variates, each represented by L tokens embedded in d dimensions, the complexity of fully self-attention models can reach unacceptably $\mathcal{O}(N^2L^2d)$ [9, 10]. As both N and L grow, such quadratic scaling becomes a major bottleneck for long-term and large-scale MTS modeling, motivating the development of more computationally efficient architectures for lightweight MTS analysis.

Recently, **Mamba** has emerged as a promising backbone for capturing complex dependencies in sequential data [26, 27, 28]. By leveraging selective mechanisms and hardware-aware computational designs [28], Mamba attains modeling performance comparable to Transformers while maintaining linear complexity with respect to sequence length. Furthermore, Mamba-2 [27] further improves effi-

ciency by exploiting the structured State Space Duality (SSD) property to reformulate computations into highly parallelizable matrix operations. With *high expressiveness* enabled by the selective mechanism, *efficient training and inference* supported by parallel computation, and *linear scalability* in context length, Mamba offers a compelling alternative to attention-based architectures for sequential modeling. Consequently, an increasing number of Mamba-based models have been proposed across various domains, such as Jamba [29] in natural language processing, Vision Mamba [30] in computer vision, Caduceus [31] in genomics, and SSD4Rec [32] for recommender systems.

Despite the recent success of Mamba-style techniques in enabling efficient MTS analysis, directly applying standard Mamba to multivariate time series often yields suboptimal performance compared with state-of-the-art methods [33]. This gap can be mainly attributed to the following limitations. (1) **Lack of cross-variate modeling:** Mamba was originally developed for language-like, essentially univariate sequences and thus lacks explicit mechanisms for capturing dependencies among multiple correlated variates. Prior studies have shown that modeling inter-variable interactions is crucial for effective MTS representation learning [11, 24, 34]. (2) **Difficulty in disentangling entangled temporal and variate contexts:** Unlike language tokens that typically lie in relatively discrete contexts, MTS observations are jointly shaped by intra-series temporal dynamics and inter-series interactions. These factors often overlap and intertwine, making it difficult for vanilla Mamba to disentangle meaningful and structured representations. (3) **Insufficient explicit modeling of lag dependencies:** Mamba relies on a recurrent hidden-state update in which each state depends primarily on the immediately preceding timestep. This design may limit its ability to explicitly capture lagged effects that are pervasive in real-world MTS, where changes in one variate can influence another only after a non-negligible delay [35, 34, 36]. For instance, in traffic forecasting, an accident in one region may not immediately affect adjacent areas; instead, its impact typically propagates through the network over several minutes. Precisely capturing such propagation delays is therefore crucial for accurate dependency modeling and reliable prediction.

Motivated by the above observations, we aim to develop a Mamba-based time-series representation backbone that simultaneously captures intricate temporal dependencies and delay-aware cross-variate interactions, while retaining Mamba’s linear-time efficiency. Toward this goal, we explicitly decompose the time-series context into (i) *intra-series temporal dynamics*, which can be learned independently and in parallel for each variate, and (ii) *inter-series interactions*, which are modeled in a delay-aware manner to learn cross-variate dependencies, as illustrated in Figure 1(a)(v).

To this end, we propose a dual-path **Delay-aware Mamba** for efficient multivariate time series analysis, namely **DeMa**. Specifically, DeMa first adaptively selects task-relevant spectra via an Adaptive Fourier Filter and decomposes the input into a *Cross-Time Component* and a *Cross-Variate Component*. These two components are then fed into stacked **DuoMNet** blocks. Each DuoMNet block contains two parallel paths, each coupled with a scan operator and a lightweight Mamba-based module. Concretely, the *Cross-Time Scan* serializes each variate along the temporal axis into a 1D sequence, which is processed by *Mamba-SSD*. This design supports MTS-independent parallel computation across variates and efficiently captures long-range temporal dependencies within each series, with computation scaling linearly with the series length. In parallel, the *Cross-Variate Scan* reorganizes tokens to emphasize inter-variable interactions at each token step. The scanned sequence is processed by *Mamba-DALA*, which integrates Delay-Aware Linear Attention (DALA) to explicitly model cross-variate dependencies with both a global correlation delay and a token-level relative delay. As a result, DeMa achieves delay-aware variate interaction modeling while preserving linear-time computation. Finally, we fuse the temporal-path and variate-path representations through a weighted fusion layer and project to task-specific outputs via lightweight heads. To sum up, our major contributions include:

- We propose **DeMa**, a dual-path Mamba-based backbone for general MTS analysis that jointly captures intra-series temporal dynamics via a temporal path and delay-aware cross-variate dependencies via a variate path. Benefiting from a linear-time state-space backbone, DeMa achieves a favorable accuracy-efficiency trade-off for long-horizon and large-scale MTS modeling.
- We introduce Mamba-SSD to model intra-series temporal dependencies within each variate. It accommodates variable-length inputs and enables series-independent, parallel modeling through block-based matrix multiplication, improving both scalability and throughput.

- We design Mamba-DALA, which integrates Delay-Aware Linear Attention to explicitly model cross-variate interactions with both global correlation delays and token-level relative delays, thereby enhancing fine-grained, delay-sensitive dependency learning.
- We conduct extensive experiments on five mainstream tasks, including long- and short-term forecasting, imputation, classification, and anomaly detection. The results demonstrate that DeMa achieves consistently strong performance across tasks while significantly reducing training time and GPU memory usage, suggesting its practicality and scalability for real-world large-scale MTS analysis.

The remainder of this paper is structured as follows. Section 2 introduces the preliminaries. Section 3 introduces the proposed model, which is evaluated and discussed in Section 4. Then, Section 5 summarizes the recent development of time series analysis. Finally, conclusions are drawn in Section 6.

2 Preliminaries

2.1 Notations and Definitions

We denote a multivariate time series (MTS) within a lookback window as $\mathcal{X} \in \mathbb{R}^{N \times T}$, where N is the number of variates and T is the number of time steps. The i -th series is $\mathcal{X}_{i,:} = \{x_{i1}, x_{i2}, \dots, x_{iT}\} \in \mathbb{R}^T$, and the multivariate observation across all variates at time t is $\mathcal{X}_{:,t} = \{x_{1t}, x_{2t}, \dots, x_{Nt}\} \in \mathbb{R}^N$.

The primary objective of this work is to learn a task-agnostic representation $\mathbf{Z} = \mathcal{F}_\Theta(\mathcal{X})$, which can be adapted to downstream tasks via task-specific heads. These tasks include point-level operations such as forecasting the future H time steps $\mathcal{Y} \in \mathbb{R}^{N \times H}$, detecting anomalies or imputing missing values in the existing series $\mathcal{Y} \in \mathbb{R}^{N \times T}$, and series-level classification task, assigning a category to the MTS among C classes, $\mathcal{Y} \in \mathbb{R}^{1 \times C}$.

2.2 Mamba

2.2.1 State Space Model (SSM)

The classical State Space Models (SSMs) describes the state evolution of a linear time-invariant system, which map input signal $\mathbf{x} = \{x(1), \dots, x(t), \dots\} \in \mathbb{R}^{L \times D} \mapsto \mathbf{y} = \{y(1), \dots, y(t), \dots\} \in \mathbb{R}^{L \times D}$ through implicit latent state $h(t) \in \mathbb{R}^{N \times D}$, where t , L , D and N indicate the time step, sequence length, channel number of the signal and state size, respectively. These models can be formulated as the following linear ordinary differential equations:

$$h'(t) = \mathbf{A}h(t) + \mathbf{B}x(t), \quad y(t) = \mathbf{C}h(t) + \mathbf{D}x(t), \quad (1)$$

where $\mathbf{A} \in \mathbb{R}^{N \times N}$ is the state transition matrix that describes how states change over time, $\mathbf{B} \in \mathbb{R}^{N \times D}$ is the input matrix that controls how inputs affect state changes, $\mathbf{C} \in \mathbb{R}^{N \times D}$ denotes the output matrix that indicates how outputs are generated based on current states and $\mathbf{D} \in \mathbb{R}^D$ represents the command coefficient that determines how inputs affect outputs directly. Most SSMs exclude the second term in the observation equation, i.e., set $\mathbf{D}x(t) = 0$, which can be recognized as a skip connection in deep learning models. The time-continuous nature poses challenges for integration into deep learning architectures. To alleviate this issue, most methods utilize the Zero-Order Hold rule [26] to discretize continuous time into K intervals, which assumes that the function value remains constant over the interval $\Delta \in \mathbb{R}^D$. The Eq. (1) can be reformulated as:

$$h_t = \bar{\mathbf{A}}h_{t-1} + \bar{\mathbf{B}}x_t, \quad y_t = \mathbf{C}h_t, \quad (2)$$

where $\bar{\mathbf{A}} = \exp(\Delta \mathbf{A})$ and $\bar{\mathbf{B}} = (\Delta \mathbf{A})^{-1}(\exp(\Delta \mathbf{A}) - \mathbf{I}) \cdot \Delta \mathbf{B}$. Discrete SSMs can be interpreted as a combination of CNNs and RNNs. Typically, the model employs a convolutional mode for efficient, parallelizable training and switches to a recurrent mode for efficient autoregressive inference. The formulations in Eq. (2) are equivalent to the following convolution [37]:

$$\begin{aligned} \bar{\mathbf{K}} &= (\mathbf{C}\bar{\mathbf{B}}, \mathbf{C}\bar{\mathbf{A}}\bar{\mathbf{B}}, \dots, \mathbf{C}\bar{\mathbf{A}}^k\bar{\mathbf{B}}, \dots), \\ \mathbf{y} &= \mathbf{x} * \bar{\mathbf{K}}, \end{aligned} \quad (3)$$

Thus, the overall process can be represented as:

$$\mathbf{y} = \text{SSM}(\bar{\mathbf{A}}, \bar{\mathbf{B}}, \mathbf{C})(\mathbf{x}). \quad (4)$$

2.2.2 Selective State Space Model (Mamba)

The discrete SSMs are based on data-independent parameters, meaning that parameters $\bar{\mathbf{A}}$, $\bar{\mathbf{B}}$, and \mathbf{C} are time-invariant and the same for any input, limiting their effectiveness in compressing context into a smaller state [26]. Mamba [26] introduces a selective mechanism to filter out extraneous information while retaining pertinent details indefinitely. Specifically, it utilizes Linear Projection to parameterize the weight matrices $\{\mathbf{B}_t\}_{t=1}^L$, $\{\mathbf{C}_t\}_{t=1}^L$ and $\{\Delta_t\}_{t=1}^L$ according to model input $\{x_t\}_{t=1}^L$, improving the context-aware ability, i.e.,:

$$\begin{aligned}\bar{\mathbf{B}}_t &= \text{Linear}_{\mathbf{B}}(x_t), \\ \bar{\mathbf{C}}_t &= \text{Linear}_{\mathbf{C}}(x_t), \\ \Delta_t &= \text{Softplus}(\text{Linear}_{\Delta}(x_t)).\end{aligned}\tag{5}$$

Then the output sequence $\{y_t\}_{t=1}^L$ can be computed with those input-adaptive discretized parameters as follows:

$$h_t = \bar{\mathbf{A}}_t h_{t-1} + \bar{\mathbf{B}}_t x_t, \quad y_t = \bar{\mathbf{C}}_t h_t.\tag{6}$$

The selection mechanism hinders SSMs from supporting parallel training like CNNs. To overcome this, Mamba adopts Parallel Associative Scan [38] and Memory Recomputation. The former exploits linear associativity and the parallelism of GPUs and TPUs for memory-efficient computation, while the latter reduces memory usage by recomputing intermediate states during backpropagation.

2.2.3 Mamba-2

Mamba-2 [27] introduces a comprehensive framework known as Structured State-Space Duality (SSD). Leveraging SSD, it reformulates SSMs as semi-separable matrices via matrix transformation and develops a more hardware-efficient computation method based on block-decomposed matrix multiplication, i.e.,

$$\begin{aligned}\mathbf{y} &= \text{SSD}(\mathbf{A}, \mathbf{B}, \mathbf{C})(\mathbf{x}) \\ &= \mathbf{M}\mathbf{x} \\ \text{s.t. } \mathbf{M} &= \begin{pmatrix} \mathbf{C}_0^\top \mathbf{A}_{0:0} \mathbf{B}_0 & & & \\ \mathbf{C}_1^\top \mathbf{A}_{1:0} \mathbf{B}_0 & \mathbf{C}_1^\top \mathbf{A}_{1:1} \mathbf{B}_1 & & \\ \dots & \dots & \dots & \dots \\ \mathbf{C}_j^\top \mathbf{A}_{j:0} \mathbf{B}_0 & \mathbf{C}_j^\top \mathbf{A}_{j:1} \mathbf{B}_1 & \dots & \mathbf{C}_j^\top \mathbf{A}_{j:i} \mathbf{B}_i \end{pmatrix}\end{aligned}\tag{7}$$

where \mathbf{M} denotes the matrix form of SSMs that uses the sequentially semiseparable representation, and $\mathbf{M}_{ji} = \mathbf{C}_j^\top \mathbf{A}_{j:i} \mathbf{B}_i$, \mathbf{C}_j and \mathbf{B}_i represent the selective space state matrices associated with input tokens x_j and x_i , respectively. $\mathbf{A}_{j:i}$ denotes the selective matrix of hidden states corresponding to the input tokens ranging from j to i . Mamba-2 achieves a 2-8 \times faster training process than Mamba-1's parallel associative scan while remaining competitive with Transformers.

3 The Proposed Method: DeMa

3.1 Structure Overview

As shown in Figure 2 (left), the proposed DeMa comprises three stages: *Adaptive Fourier Filter*, the stacked *DuoMNet blocks*, and *Task-specific Projection*. First, the Adaptive Fourier Filter module filters and distangles the input raw MTS into intra-series temporal dynamics components and inter-series interactions components. Then, these two components are fed into the stacked DuoMNet Blocks. Each DuoMNet Block, as shown in Figure 2 (right), takes the residual of the previous block's fitted dynamics as its input, and learn temporal dependencies and variate dependencies through a temporal path and a variate path, respectively. Finally, task-specific projection layers will be utilized to tailor the model for various time series analysis tasks, including forecasting, imputation, classification, and anomaly detection.

3.1.1 Adaptive Fourier Filter

Real-world multivariate time series often exhibit overlapping and entangled patterns arising from (i) *intra-series temporal dynamics* within each variate and (ii) *inter-series interactions* among

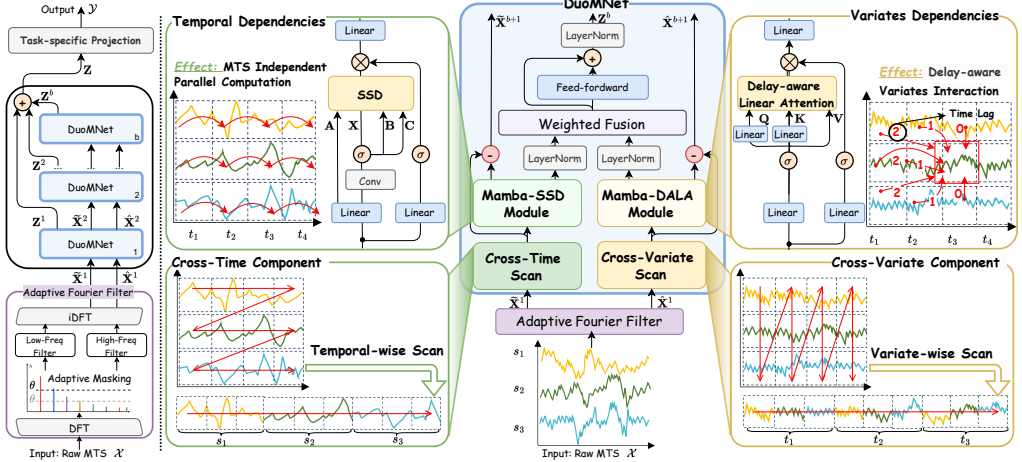


Figure 2: The overall framework of DeMa. The proposed DeMa (Left) comprises three key components: Adaptive Fourier Filter and stacked DuoMNet Blocks, and Task-specific Projection. Most importantly, the DuoMNet Block (Right) integrates insights from the Mamba-SSD path and the Mamba-DALA path to achieve comprehensive modeling of cross-time and cross-variate dependencies.

correlated variates. In the frequency domain, slowly varying structures such as trends and seasonal cycles are typically concentrated in low-frequency bands, whereas short-term variations, including abrupt changes and time-varying cross-variate effects, tend to appear at higher frequencies [39, 40]. Meanwhile, different tasks emphasize different spectral contents: numerical prediction tasks (such as forecasting, imputation, and anomaly detection) are usually sensitive to local dynamics, whereas semantic tasks (e.g., classification) rely more on global and long-range patterns [41]. These characteristics motivate a task-adaptive spectral decomposition that separates and highlights task-relevant components.

To facilitate modeling of intra-series dynamics and inter-series interactions, we split the input into two complementary frequency subsets. The *globally dominant* frequencies capture broadly shared, long-term structures and mainly reflect per-variate temporal dynamics, while the *residual* frequencies encode more window-specific variations that are often indicative of time-varying cross-variate interactions. Concretely, given an input window $\mathcal{X} \in \mathbb{R}^{N \times T}$ with length T , we first apply the Fast Fourier Transform (FFT) along the temporal axis for each variate and obtain the averaged amplitude for each frequency index in $\mathcal{S} = \{0, 1, \dots, \lfloor T/2 \rfloor\}$. We rank \mathcal{S} by amplitude, select the top θ fraction as \mathcal{S}_θ , and denote the complement by $\overline{\mathcal{S}}_\theta = \mathcal{S} \setminus \mathcal{S}_\theta$. The Adaptive Fourier Filter $\text{AFF}(\cdot)$ then decomposes \mathcal{X} as

$$\begin{aligned} \text{Cross-Time Component} : \tilde{\mathcal{X}} &= \text{FFT}^{-1} \left(\text{Filter} (\mathcal{S}_\theta, \text{FFT}(\mathcal{X})) \right), \\ \text{Cross-Variate Component} : \hat{\mathcal{X}} &= \text{FFT}^{-1} \left(\text{Filter} (\overline{\mathcal{S}}_\theta, \text{FFT}(\mathcal{X})) \right), \end{aligned} \quad (8)$$

where FFT^{-1} denotes the inverse FFT and $\text{Filter}(\cdot)$ retains only the coefficients indexed by the specified set. The *Cross-Time Component* $\tilde{\mathcal{X}}$ is dominated by global, low-frequency spectral components that primarily reflect intra-series temporal dynamics, and *Cross-Variate Component* $\hat{\mathcal{X}}$ preserves the remaining variations, typically higher-frequency and window-specific, which are related to inter-series interactions.

This decomposition is particularly valuable when a state space model is used as the backbone for MTS modeling. In Mamba, the HiPPO-based state-space formulation has been shown to induce approximately orthogonal transformations [42]. However, orthogonality of the learned transform does not imply that mixed components in raw MTS can be cleanly separated: if two underlying components are *not* orthogonal in the input space, their projections onto any orthogonal basis must share some basis directions. We formalize this limitation below.

Theorem 1 (Non-orthogonality implies basis overlap). *Given the input series $\mathcal{X} = \tilde{\mathcal{X}} + \hat{\mathcal{X}}$ and let $E = \{e_1, \dots, e_N\}$ be an orthogonal basis. Suppose*

$$\tilde{\mathcal{X}} = \sum_{i=1}^N a_i e_i, \quad \hat{\mathcal{X}} = \sum_{i=1}^N b_i e_i,$$

and define the supports $\tilde{E} = \{e_i \in E : a_i \neq 0\}$ and $\hat{E} = \{e_i \in E : b_i \neq 0\}$. If $\tilde{\mathcal{X}}$ and $\hat{\mathcal{X}}$ are not orthogonal, i.e., $\langle \tilde{\mathcal{X}}, \hat{\mathcal{X}} \rangle \neq 0$, then $\tilde{E} \cap \hat{E} \neq \emptyset$. Equivalently, two non-orthogonal components cannot be represented on disjoint subsets of an orthogonal basis.

Proof. Since $E = \{e_1, \dots, e_N\}$ is an orthogonal basis, we have $\langle e_i, e_j \rangle = 0$ for $i \neq j$ and $\langle e_i, e_i \rangle > 0$ for all i . Thus,

$$\begin{aligned} \langle \tilde{\mathcal{X}}, \hat{\mathcal{X}} \rangle &= \left\langle \sum_{i=1}^N a_i e_i, \sum_{j=1}^N b_j e_j \right\rangle \\ &= \sum_{i=1}^N \sum_{j=1}^N a_i b_j \langle e_i, e_j \rangle \\ &= \sum_{i=1}^N a_i b_i \langle e_i, e_i \rangle, \end{aligned} \tag{9}$$

If $\tilde{E} \cap \hat{E} = \emptyset$, then for every i at least one of a_i or b_i is zero, implying $a_i b_i = 0$ for all i , which implies

$$\langle \tilde{\mathcal{X}}, \hat{\mathcal{X}} \rangle = \sum_{i=1}^N a_i b_i \langle e_i, e_i \rangle = 0. \tag{10}$$

This contradicts the assumption $\langle \tilde{\mathcal{X}}, \hat{\mathcal{X}} \rangle \neq 0$. Therefore, there exists at least one index i such that $a_i \neq 0$ and $b_i \neq 0$, i.e., $e_i \in \tilde{E} \cap \hat{E}$. \square

Theorem 1 implies that if the Cross-Time component $\tilde{\mathcal{X}}$ and the Cross-Variate component $\hat{\mathcal{X}}$ are non-orthogonal, their representations on any orthogonal basis must overlap, making a complete separation by an orthogonal transform impossible. In practice, this non-orthogonality often arises because different generative factors are *not* confined to disjoint frequency bands: for example, trend, seasonality, and interaction-driven fluctuations can partially share the same spectral range and thus superimpose in both time and frequency domains. Therefore, although HiPPO-based SSMs tend to learn orthogonal transformations [42], applying a single Mamba model directly to raw MTS may still entangle these factors. In contrast, our proposed AFF(\cdot) explicitly decomposes \mathcal{X} into complementary spectral parts, allowing subsequent modules to model them separately and thereby reducing representational entanglement and avoiding redundant modeling capacity.

3.2 DuoMNet Block

In this section, we detail the design of the proposed DuoMNet block, which consists of a temporal path to capture cross-time dependencies and a variate path to learn cross-variate dependencies, respectively.

3.2.1 Cross-Time Scan and Cross-Variate Scan

Given the decomposed Cross-Time Component $\tilde{\mathcal{X}} \in \mathbb{R}^{N \times T}$ and Cross-Variate Component $\hat{\mathcal{X}} \in \mathbb{R}^{N \times T}$, we tokenize each component into patch tokens to reduce point-wise redundancy and encode local temporal semantics [8, 24]. Concretely, for each variate i , we apply reversible instance normalization (RevIN) [43] and partition the normalized series into L contiguous patches of length P . A lightweight 1-D convolutional encoder maps each patch to a D -dimensional embedding. To enable complementary dependency modeling, we organize the resulting embeddings with two scan orders:

(a) **Cross-Time Scan (temporal-wise).** We preserve the temporal order of patch tokens in the Cross-Time Component and stack all variates in parallel:

$$\tilde{\mathbf{X}} = [\tilde{\mathbf{X}}_{1,:}; \tilde{\mathbf{X}}_{2,:}; \dots; \tilde{\mathbf{X}}_{N,:}] \in \mathbb{R}^{N \times L \times D}, \quad (11)$$

where $\tilde{\mathbf{X}}_{i,:} \in \mathbb{R}^{L \times D}$ contains the L patch embeddings of the i -th variate. This scan order enables the temporal module to model *intra-series* dependencies along the temporal axis independently for each variate.

(b) **Cross-Variate Scan (variety-wise).** We instead group tokens in the Cross-Variate Component by the same patch position and scan across variates:

$$\hat{\mathbf{X}} = (\hat{\mathbf{X}}_{:,1}, \hat{\mathbf{X}}_{:,2}, \dots, \hat{\mathbf{X}}_{:,L}) \in \mathbb{R}^{L \times N \times D}, \quad (12)$$

where $\hat{\mathbf{X}}_{:,l} = (\hat{\mathbf{x}}_{1,l}, \dots, \hat{\mathbf{x}}_{N,l}) \in \mathbb{R}^{N \times D}$ collects the embeddings of all N variates at the l -th token step. This scan order preserves the chronological order over token indices and facilitates modeling time-varying cross-variate interactions at different token steps.

These two scanned representations, $\tilde{\mathbf{X}}$ and $\hat{\mathbf{X}}$, are then fed into subsequent modules to learn cross-time and cross-variate dependencies, respectively.

3.2.2 Cross-Time Dependencies Modeling via Mamba-SSD

Given the temporal-wise scanned embeddings $\tilde{\mathbf{X}} \in \mathbb{R}^{N \times L \times D}$ of the Cross-Time component, our goal is to capture *intra-series* temporal dependencies within each variate. We therefore adopt an **independent and parallel** strategy: each variate is modeled without cross-variate coupling, enabling efficient parallel computation across N variates. The proposed Mamba-SSD module consists of four stages: (a) two-branch gating and local mixing, (b) selective SSM parameterization, (c) Structured State Duality (SSD) based parallel scan, and (d) gated output projection.

(a) **Two-branch Gating and Local Mixing.** We first apply linear projections to obtain a content branch $\tilde{\mathbf{X}} \in \mathbb{R}^{N \times L \times D_u}$ and a gate branch $\tilde{\mathbf{X}}_{\text{gate}} \in \mathbb{R}^{N \times L \times D_u}$. The gate branch serves as a residual controller that adaptively filters and reweights the content features. We then perform local temporal mixing by applying a lightweight 1-D convolution along the token axis on the content branch (for each variate in parallel), which injects an explicit short-range inductive bias to model local continuity that is common in real-world time series, and complements the long-range selective SSM by providing locally aggregated features that stabilize token-dependent parameter generation.

(b) **Selective SSM parameterization.** Following Mamba-style selective SSMs, we generate token-dependent parameters from $\tilde{\mathbf{X}}$. Let D_h denote the state dimension. The step size and the output projections are computed as

$$\begin{aligned} \Delta &= \text{softplus}(\tilde{\mathbf{X}} \mathbf{W}_\Delta + \mathbf{b}_\Delta) \in \mathbb{R}^{N \times L \times D_h}, \\ \mathbf{B} &= \tilde{\mathbf{X}} \mathbf{W}_B + \mathbf{b}_B \in \mathbb{R}^{N \times L \times D_h}, \\ \mathbf{C} &= \tilde{\mathbf{X}} \mathbf{W}_C + \mathbf{b}_C \in \mathbb{R}^{N \times L \times D_h}, \end{aligned} \quad (13)$$

where $\mathbf{W}_\Delta, \mathbf{W}_B, \mathbf{W}_C \in \mathbb{R}^{D_u \times D_h}$. To ensure stable dynamics, we parameterize the continuous-time transition with a negative diagonal vector $\mathbf{A} = -\exp(\mathbf{A}_{\log}) \in \mathbb{R}^{D_h}$ and discretize it using Δ :

$$\begin{aligned} \bar{\mathbf{A}} &= \exp(\Delta \odot \mathbf{A}) \in \mathbb{R}^{N \times L \times D_h}, \\ \bar{\mathbf{B}} &= (1 - \bar{\mathbf{A}}) \odot \mathbf{B} \in \mathbb{R}^{N \times L \times D_h}, \end{aligned} \quad (14)$$

where \odot denotes element-wise multiplication. Here, Δ controls the effective memory scale at each token, while \mathbf{B} and \mathbf{C} modulate how content is written into and read from the latent state, yielding content-adaptive dynamics.

(c) **SSD-based Parallel Computation.** Given the input token sequence $\tilde{\mathbf{X}} \in \mathbb{R}^{N \times L \times D_u}$, the selective SSM at step t can be formulated as follows:

$$\begin{aligned} h_t &= \bar{\mathbf{A}}_t h_{t-1} + \bar{\mathbf{B}}_t \tilde{\mathbf{X}}_t, \\ \mathbf{Y}_t &= \mathbf{C}_t^\top h_t, \end{aligned} \quad (15)$$

which yields $\mathbf{Y} \in \mathbb{R}^{N \times L \times D_h}$. Equivalently, the induced linear operator is *block-diagonal* across variates by leveraging Structured State-Space Duality (SSD) properties in Mamba-2 [27]. Specifically, the selective SSM model presented in Eq. (15) can be reformulated as:

$$\begin{aligned} \mathbf{Y}_{\text{time}} &= \text{SSD}(\mathbf{A}, \mathbf{B}, \mathbf{C})(\tilde{\mathbf{X}}) = \mathbf{M}\tilde{\mathbf{X}} \\ \text{s.t. } \mathbf{M} &= \begin{pmatrix} \mathbf{C}_0^\top \mathbf{A}_{0:0} \mathbf{B}_0 & & & \\ \mathbf{C}_1^\top \mathbf{A}_{1:0} \mathbf{B}_0 & \mathbf{C}_1^\top \mathbf{A}_{1:1} \mathbf{B}_1 & & \\ \cdots & \cdots & \cdots & \cdots \\ \mathbf{C}_j^\top \mathbf{A}_{j:0} \mathbf{B}_0 & \mathbf{C}_j^\top \mathbf{A}_{j:1} \mathbf{B}_1 & \cdots & \mathbf{C}_j^\top \mathbf{A}_{j:i} \mathbf{B}_i \end{pmatrix}, \end{aligned} \quad (16)$$

where \mathbf{M} denotes the matrix form of SSMs that uses the sequentially semiseparable representation, and $\mathbf{M}_{ji} = \mathbf{C}_j^\top \mathbf{A}_{j:i} \mathbf{B}_i$ represents the mapping from the i -th input token to the j -th output token. Here, \mathbf{B}_i and \mathbf{C}_j are the selective state-space parameters associated with the i -th and j -th tokens, respectively, and $\mathbf{A}_{j:i}$ denotes the product of the transition terms from step i to j .

By representing state space models as semiseparable matrices through matrix transformations, the structured state-space model enables block-based matrix multiplication, allowing for content-aware modeling analogous to attention while achieving subquadratic-time computation. Building on this insight, we perform the SSD operator in parallel over all N variates:

$$\begin{aligned} \mathbf{Y}_{\text{time}} &= \text{SSD}(\mathbf{A}, \mathbf{B}, \mathbf{C})(\tilde{\mathbf{X}}) \\ &= (\mathbf{M}_1 \tilde{\mathbf{X}}_{1,:}; \mathbf{M}_2 \tilde{\mathbf{X}}_{2,:}; \dots; \mathbf{M}_N \tilde{\mathbf{X}}_{N,:}), \end{aligned} \quad (17)$$

where each \mathbf{M}_n is a semiseparable operator acting only on the n -th variate sequence. Notably, during this process, we prevent any cross-series information flow by re-initializing (i.e., zeroing) the hidden state at the beginning of each series, thereby forcing the Mamba-SSD path to focus exclusively on temporal modeling. This explicitly enforces that the Cross-Time branch captures temporal dynamics *within* each variate while remaining fully parallelizable across N variates.

(d) **Gated Output Projection.** Finally, we combine the SSD output \mathbf{Y}_{time} from the content branch with the gate branch to obtain the final output:

$$\tilde{\mathbf{Y}} = \text{Linear}(\mathbf{Y}_{\text{time}} \odot \sigma(\tilde{\mathbf{X}}_{\text{gate}})), \quad (18)$$

where $\sigma(\cdot)$ is the sigmoid function and \odot denotes element-wise multiplication. The purpose of this gated projection is to provide an explicit, token-adaptive modulation on the propagated state features, selectively enhancing informative temporal responses while attenuating irrelevant or noisy activations, thereby improving robustness and expressiveness without introducing cross-variational coupling. Thus, the overall process in the Mamba-SSD module is:

$$\tilde{\mathbf{Y}} = \text{Mamba-SSD}(\tilde{\mathbf{X}}). \quad (19)$$

3.2.3 Cross-Variate Dependencies Modeling via Mamba-DALA

A critical yet often overlooked factor in multivariate time series modeling is the *delay dependency*: variations in one variate may influence another only after a *time lag* [35, 3]. For instance, in traffic forecasting, congestion at an intersection typically propagates to nearby intersections with a non-negligible delay rather than instantaneously. This lagged propagation property makes forecasting more challenging. Accurately capturing such delayed interactions is essential for both predictive performance and practical utility, yet this effect is often overlooked in existing time series models.

To efficiently capture cross-variante dependencies in the Cross-Variate component $\hat{\mathbf{X}} \in \mathbb{R}^{L \times N \times D}$ while explicitly accounting for delay effect, we develop a Mamba-style mixing block that replaces the recurrent SSM in the Mamba backbone with a **Delay-Aware Linear Attention (DALA)** operator, termed **Mamba-DALA**. Built upon Mamba’s efficient block design [44], Mamba-DALA performs token-wise pairwise interaction modeling across variates, yielding delay-aware cross-variante aggregation among multiple correlated latent series.

(a) **Mamba-style Gating and Parameterization.** Following the two-branch design in Mamba, we apply linear projections to obtain a content branch $\hat{\mathbf{X}} \in \mathbb{R}^{L \times N \times D_u}$ and a gate branch $\hat{\mathbf{X}}_{\text{gate}} \in \mathbb{R}^{L \times N \times D_u}$. We further construct the linear-attention operator by $\hat{\mathbf{X}}^q = \hat{\mathbf{X}} \mathbf{W}_Q$, $\hat{\mathbf{X}}^k = \hat{\mathbf{X}} \mathbf{W}_K$, $\hat{\mathbf{X}}^v = \hat{\mathbf{X}} \mathbf{W}_V$, where $\mathbf{W}_Q, \mathbf{W}_K, \mathbf{W}_V \in \mathbb{R}^{D_u \times D_u}$.

(b) **Delay-Aware Linear Attention (DALA).** To robustly encode propagation delays, we consider two delay signals: a *global correlation delay* and a *token-level relative delay*. The motivation is to correct the coarse-grained cross-series misalignment via global offset, and explicitly consider the token-wise temporal relative distance between interacting tokens, so that we can both correct the most plausible alignment shift and preserve ordered, causal interactions at the token level. Accordingly, we first estimate the correlation delay by maximizing the cross-correlation between variates, which serves as an explicit prior for cross-series alignment. After compensating for this global offset, we further leverage the token-level relative delay encoded by Rotary Position Embedding (RoPE) [45] to capture time lags between query-key token pairs.

Global correlation delay. we first estimate the global propagation delay by maximizing the cross-correlation [46] between latent correlated series $\mathcal{X}_{a,:} \in \mathbb{R}^T$ and $\mathcal{X}_{b,:} \in \mathbb{R}^T$ via temporal shifting [35]. Meanwhile, we quantify the *correlation strength* as the peak correlation value:

$$\begin{aligned}\tau_{ab} &= \arg \max_t \text{corr}(\mathcal{X}_{a,:} \xrightarrow{t} \mathcal{X}_{b,:}), \\ \rho_{ab} &= \text{corr}(\mathcal{X}_{a,:} \xrightarrow{\tau_{ab}} \mathcal{X}_{b,:}),\end{aligned}\quad (20)$$

where \xrightarrow{t} denotes a t -step shift applied to $\mathcal{X}_{a,:}$, and $\text{corr}(\cdot)$ represents the Pearson correlation function. The strength ρ_{ab} is used to weight cross-variate aggregation, so that more strongly correlated pairs contribute more. Since τ_{ab} is defined in the original time point scale, we map it to the token scale as an integer shift:

$$\Delta_{ab} = \text{round}\left(\frac{\tau_{ab}}{P}\right) \in \mathbb{Z}, \quad (21)$$

where P is the time points per token, $\Delta_{ab} > 0$ indicates that series a lags behind series b on the token scale.

Token-level relative delay. For a query token $\hat{\mathbf{X}}_{a,l}^q$ at position l and a key token $\hat{\mathbf{X}}_{b,j}$ at position j , RoPE parameterizes their token-wise relative delay $(l - j)$ by:

$$\mathcal{R}_{l-j}^\Theta = \mathcal{R}_l^\Theta (\mathcal{R}_j^\Theta)^T, \quad (22)$$

where \mathcal{R}_l^Θ and \mathcal{R}_j^Θ denote rotary position embeddings for the l -th and j -th tokens, and Θ is the shared predefined RoPE parameterization [45]. To incorporate the global token shift, we align the key token $\hat{\mathbf{X}}_{b,j}$ from series b to the effective position $j + \Delta_{ab}$ when interacting with series a . Consequently, the query-key interaction is governed by a unified effective delay:

$$\delta_{l,j}^{a \leftarrow b} = l - (j + \Delta_{ab}) = (l - j) - \Delta_{ab}, \quad (23)$$

which simultaneously accounts for the global propagation offset and the local token-wise lag.

Delay-aware attention aggregation. Given a query token $\hat{\mathbf{X}}_{a,l}^q$ at position l in series a , we allow it to attend to key tokens $\hat{\mathbf{X}}_{b,j}^k$ from all variates $b \in \{1, \dots, N\}$, while enforcing the causal constraint $j + \Delta_{ab} \leq l$ to prevent information leakage. We inject the effective delay by applying RoPE for query at positions l and for key at $j + \Delta_{ab}$, yielding \mathcal{R}_l^Θ and $\mathcal{R}_{j+\Delta_{ab}}^\Theta$, respectively. The delay-aware linear attention output $\mathbf{y}_{a,l} \in \mathbb{R}^{D_u}$ is computed as

$$\mathbf{y}_{a,l} = \mathcal{R}_l^\Theta \phi(\hat{\mathbf{X}}_{a,l}^q) \frac{\sum_{b=1}^N \rho_{ab} \sum_{j:j+\Delta_{ab} \leq l} (\mathcal{R}_{j+\Delta_{ab}}^\Theta \phi(\hat{\mathbf{X}}_{b,j}^k))^T \hat{\mathbf{X}}_{b,j}^v}{\phi(\hat{\mathbf{X}}_{a,l}^q) \sum_{b=1}^N \rho_{ab} \sum_{j:j+\Delta_{ab} \leq l} \phi(\hat{\mathbf{X}}_{b,j}^k)^T}, \quad (24)$$

where $\phi(\cdot)$ is the kernel function in [47], i.e., $\phi(x) = f(\text{ReLU}(x))$ with $f(x) = \frac{\|x\|}{\|x\|^{**p}} x^{**p}$ and x^{**p} denoting the element-wise power p . This kernelization enhances the expressiveness of linear attention by amplifying informative query-key similarity patterns, while ρ_{ab} further emphasizes reliable cross-variate interactions. Applying Eq. (24) to all tokens yields the DALA output to all patched tokens in $\hat{\mathbf{X}}$ to uncover all the cross-variate dependencies among series to obtain the DALA output $\mathbf{Y}_{\text{variate}} \in \mathbb{R}^{L \times N \times D_u}$.

(c) **Gated Output Projection.** Following Mamba’s gated mixing, we modulate $\mathbf{Y}_{\text{variate}}$ with the gate branch $\hat{\mathbf{X}}_{\text{gate}} \in \mathbb{R}^{L \times N \times D_u}$ via an element-wise multiplicative gate, and project it back to the model dimension:

$$\hat{\mathbf{Y}} = \text{Linear}(\mathbf{Y}_{\text{variate}} \odot \sigma(\hat{\mathbf{X}}_{\text{gate}})), \quad (25)$$

where \odot denotes element-wise multiplication and $\sigma(\cdot)$ is the gating activation. Thus, the overall process in the Mamba-DALA module is summarized as:

$$\hat{\mathbf{Y}} = \text{Mamba-DALA}(\hat{\mathbf{X}}). \quad (26)$$

3.2.4 DuoMNet Block Design

As illustrated in Fig. 2, each **DuoMNet** block consists of two complementary paths: (i) a *temporal path* implemented by Mamba-SSD to capture cross-time dependencies, and (ii) a *variety path* implemented by Mamba-DALA to model delay-aware cross-variate dependencies. We update the input $\tilde{\mathbf{X}}^{b+1}$ and $\hat{\mathbf{X}}^{b+1}$ of both paths via residual connections and pass them to the next block:

$$\begin{aligned} \tilde{\mathbf{X}}^{b+1} &= \tilde{\mathbf{X}}^b - \tilde{\mathbf{Y}}^b = \tilde{\mathbf{X}}^b - \text{Mamba-SSD}(\tilde{\mathbf{X}}^b), \\ \hat{\mathbf{X}}^{b+1} &= \hat{\mathbf{X}}^b - \hat{\mathbf{Y}}^b = \hat{\mathbf{X}}^b - \text{Mamba-DALA}(\hat{\mathbf{X}}^b). \end{aligned} \quad (27)$$

To integrate the two complementary outputs, we first apply LayerNorm to each path and then perform a weighted fusion:

$$\mathbf{U}^b = \alpha \text{ LN}(\tilde{\mathbf{Y}}^b) + \beta \text{ LN}(\hat{\mathbf{Y}}^b), \quad (28)$$

where α and β are mixing hyperparameters. We then apply a feed-forward network (FFN) to the mixed representation and use a residual connection followed by LN to obtain the block output:

$$\mathbf{Z}^b = \text{LN}(\mathbf{U}^b + \text{FFN}(\mathbf{U}^b)). \quad (29)$$

Here, \mathbf{Z}^b is the output of the b -th DuoMNet block. By stacking B DuoMNet blocks, we obtain $\{\mathbf{Z}^b\}_{b=1}^B$. Following a layer-wise aggregation strategy, the final representation is computed as:

$$\mathbf{Z} = \sum_{b=1}^B \mathbf{Z}^b. \quad (30)$$

3.3 Task-specific Projection

To adapt DeMa to diverse downstream tasks (e.g., forecasting, imputation, anomaly detection, and classification), we attach a lightweight task head on top of the final task-agnostic representation $\mathbf{Z} \in \mathbb{R}^{N \times L \times D}$ to learn task-specific targets. For regression-oriented tasks such as forecasting, imputation, and anomaly detection, we employ an MLP as the task head $\mathcal{Y} = \text{MLP}(\mathbf{Z})$. For forecasting, the prediction is $\mathcal{Y} \in \mathbb{R}^{N \times S}$, where S is the prediction horizon. For imputation and anomaly detection, the head produces point-wise outputs over the lookback window, i.e., $\mathcal{Y} \in \mathbb{R}^{N \times T}$, where T is the lookback length. For series-level classification, we first aggregate token-wise representations into a global feature, and then apply an MLP classifier with softmax $\mathcal{Y} = \text{softmax}(\text{MLP}(\mathbf{Z}))$, where $\mathcal{Y} \in \mathbb{R}^{1 \times C}$ and C is the number of classes.

3.4 Training Process and Complexity Analysis

The overall training procedure is summarized in Algorithm 1. The computational cost of DeMa is dominated by two parallel modules, Mamba-SSD and Mamba-DALA. Let L be the number of patches and D the model dimension. For Mamba-SSD, the Cross-Time scan yields $\tilde{\mathbf{X}} \in \mathbb{R}^{N \times L \times D}$, which can be viewed as a scanned sequence of length NL for SSD-based selective state-space computation. The resulting FLOPs scale linearly with the scanned length and quadratically with the feature dimension, giving a per-block complexity of $\mathcal{O}((NL)D^2)$. Similarly, Mamba-DALA operates on $\hat{\mathbf{X}} \in \mathbb{R}^{L \times N \times D}$, which can equivalently be viewed as a sequence of length LN . Its core delay-aware linear mixing is implemented via linear attention and thus also requires $\mathcal{O}((LN)D^2)$ FLOPs per block. Since the two paths are computed in parallel, the overall complexity per DuoMNet block remains $\mathcal{O}((NL)D^2)$. Consequently, DeMa achieves linear-time complexity with respect to the effective scanned length NL , enabling efficient modeling for long-horizon and large-scale multivariate time series in regimes where the effective token length dominates the feature dimension, i.e., $N, L \gg D$.

Algorithm 1: DeMa

Input: Raw MTS window $\mathcal{X} \in \mathbb{R}^{N \times T}$; top-ratio θ ; patch length P ; #blocks B ; fusion weights (α, β) ; task head $\text{MLP}(\cdot)$.

Output: Task output \mathcal{Y} and model \mathcal{F}_Θ .

```
/* Adaptive Fourier Filter (AFF) */  
( $\tilde{\mathcal{X}}, \hat{\mathcal{X}}$ )  $\leftarrow$  AFF( $\mathcal{X}; \theta$ ) (Eq. (8)); /*  
/* Tokenization + Scan */  
 $\tilde{\mathbf{X}}^1 \leftarrow$  CrossTimeScan(PatchEmbed( $\tilde{\mathcal{X}}; P$ ))  $\in \mathbb{R}^{N \times L \times D}$ ;  
 $\hat{\mathbf{X}}^1 \leftarrow$  CrossVariateScan(PatchEmbed( $\hat{\mathcal{X}}; P$ ))  $\in \mathbb{R}^{L \times N \times D}$ ;  
/* Delay priors */  
Compute  $(\tau_{ab}, \rho_{ab})$  by Eq. (20) and  $\Delta_{ab}$  by Eq. (21) for all series pair  $(a, b)$ ;  
/* Stacked DuoMNet Blocks */  
for  $b = 1, 2, \dots, B$  do /*  
/* Parallel paths (Temporal & Variate) */  
 $\tilde{\mathbf{Y}}^b \leftarrow$  Mamba-SSD( $\tilde{\mathbf{X}}^b$ ) (Eqs. (13)- (19));  
 $\hat{\mathbf{Y}}^b \leftarrow$  Mamba-DALA( $\hat{\mathbf{X}}^b; \{\Delta_{ab}\}, \{\rho_{ab}\}$ ) (Eqs. (23)- (26)); /*  
/* Residual update */  
 $(\tilde{\mathbf{X}}^{b+1}, \hat{\mathbf{X}}^{b+1}) \leftarrow (\tilde{\mathbf{X}}^b - \tilde{\mathbf{Y}}^b, \hat{\mathbf{X}}^b - \hat{\mathbf{Y}}^b)$  (Eq. (27)); /*  
/* Fusion + FFN */  
 $\mathbf{U}^b \leftarrow \alpha \text{LN}(\tilde{\mathbf{Y}}^b) + \beta \text{LN}(\hat{\mathbf{Y}}^b)$  (Eq. (28));  
 $\mathbf{Z}^b \leftarrow \text{LN}(\mathbf{U}^b + \text{FFN}(\mathbf{U}^b))$  (Eq. (29)); /*  
/* Aggregation + Task head */  
 $\mathbf{Z} \leftarrow \sum_{b=1}^B \mathbf{Z}^b$  (Eq. (30));  
 $\mathcal{Y} \leftarrow \text{MLP}(\mathbf{Z})$ ;  
return  $\mathcal{Y}, \mathcal{F}_\Theta$ 
```

4 Experiments

In this section, we investigate the following research questions to validate the effectiveness, efficiency, and scalability of DeMa:

- **RQ1:** How does DeMa perform across five representative time series tasks?
- **RQ2:** Does DeMa achieve a favorable accuracy-efficiency trade-off as a general backbone for multivariate time-series analysis?
- **RQ3:** How does DeMa scale with increasing input length in terms of per-iteration runtime and GPU memory, compared with Transformer-based baselines?
- **RQ4:** How does each key component contribute to the overall performance of DeMa?
- **RQ5:** How sensitive is DeMa to major hyperparameters?

4.1 Experimental Setup

4.1.1 Datasets

To validate the effectiveness of DeMa, we conduct extensive experiments on five mainstream time-series analysis tasks, including long-term forecasting, short-term forecasting, imputation, classification, and anomaly detection. All datasets are drawn from the benchmark collections in the Time Series Library (TSLib) [33]. Table 1 summarizes the datasets used for each task.

- *Forecasting.* We evaluate both long-term and short-term forecasting. For long-term forecasting, we adopt widely used benchmarks including Electricity [48], ETT with four subsets (ETTh1, ETTh2, ETTm1, ETTm2) [20], Exchange [49], Traffic [22], Weather [22], and Solar-Energy [49]. For short-term forecasting, we use four traffic datasets from the PEMS family [50]: PEMS03, PEMS04, PEMS07, and PEMS08.

Table 1: Summary of Experimental Datasets. #Variates denotes the number of variables in each multivariate time series, and #Timesteps denotes the total number of time steps.

Task	Dataset	#Variates	#Timestep	Frequency	Domain
Long-term Forecasting	ETTh1, ETTh2	7	17,420	1 hour	Electricity
	ETTm1, ETTm2	7	69,680	15 mins	Electricity
	Electricity	321	26,304	1 hour	Electricity
	Weather	21	52,696	10 mins	Environment
	Traffic	862	17,544	1 hour	Transportation
	Exchange	8	7,588	1 day	Economic
Short-term Forecasting	Solar-Energy	137	966	1 week	Health
	PEMS03	358	6	5min	Transportation
	PEMS04	307	8	5min	Transportation
	PEMS07	883	18	5min	Transportation
Imputation	PEMS08	170	13	5min	Transportation
	ETTh1, ETTh2	7	17,420	1 hour	Electricity
	ETTm1, ETTm2	7	69,680	15 mins	Electricity
	Electricity	321	26,304	1 hour	Electricity
Anomaly Detection	Weather	21	52,696	10 mins	Environment
	SMD	38	100	1 min	Industry
	MSL	55	100	1 min	Industry
	SMAP	25	100	1 min	Industry
	SWaT	51	100	1 min	Industry
Classification	PSM	25	100	1 min	Industry
	EthanolConcentration	3	1,751	-	Alcohol Industry
	FaceDetection	144	62	250 Hz	Face
	Handwriting	3	152	-	Motion
	Heartbeat	61	405	0.061 secs	Health
	JapaneseVowels	12	29	-	Voice
	PEMS-SF	963	144	1 day	Transportation
	SelfRegulationSCP1	6	896	256 Hz	Health
	SelfRegulationSCP2	7	1,152	256 Hz	Health
	SpokenArabicDigits	13	93	11025 Hz	Voice
	UWaveGestureLibrary	3	315	-	Gesture

- *Imputation.* Time-series imputation aims to recover missing values from contextual observations. We evaluate on ETTh1, ETTh2, ETTm1, ETTm2, Electricity, and Weather. Following TimesNet [12], we randomly mask time points with ratios in $\{12.5\%, 25\%, 37.5\%, 50\%\}$ to assess robustness under varying missing rates.
- *Anomaly Detection.* Anomaly detection aims to identify abnormal patterns in time series. We adopt five widely used industrial benchmarks: Server Machine Dataset (SMD) [51], Mars Science Laboratory rover (MSL) [52], Soil Moisture Active Passive satellite (SMAP) [52], Secure Water Treatment (SWaT) [53], and Pooled Server Metrics (PSM) [54].
- *Classification.* For time-series classification, we use ten multivariate datasets from the UEA Time Series Classification Archive [55], covering diverse domains such as gesture recognition, action recognition, audio recognition, and medical diagnosis.

4.1.2 Baselines.

To ensure a comprehensive comparison, we include a broad set of strong baselines that are representative of the latest advances in the time series community. Specifically, our baselines span four families: (1) Mamba-based models: Affirm [56], S-Mamba [57], CMamba [58], and SAMBA [59]; (2) Transformer-based models: iTransformer [11], Crossformer [24], and PatchTST [8]; (3) MLP-based models: TimeMixer [19], DLinear [18], and RLinear [60]; and (4) TCN-based models: ModernTCN [17] and TimesNet [12].

4.2 Metrics and Implementation Details

To ensure a fair and comprehensive comparison, we follow the experimental protocol of the well-established Time Series Library [33]. For long-term forecasting and imputation, we report mean squared error (MSE) and mean absolute error (MAE). For time-series classification, we report accuracy. For anomaly detection, we report the F1-score, which balances precision and recall and is well-suited to the highly imbalanced nature of anomalous events. In each table, the best and second-best results are highlighted in **red** and **underlined**, respectively.

We use the published optimal hyperparameter settings for all baselines. All experiments are implemented in PyTorch and conducted on three NVIDIA RTX A6000 GPUs (48GB). We train all models with the Adam optimizer [61] under an ℓ_2 loss, and tune the initial learning rate in $\{1e-4, .5e-4, .1e-3\}$. The number of DuoMNet blocks is selected from $\{2, 3, 4, 5\}$ via hyperparameter search, and the representation dimension is chosen from $\{32, 64, 128, 256\}$. We set the batch size to 32 and train for 50 epochs. We further conduct a grid search over the fusion weights $\alpha, \beta \in \{0.2, 0.4, 0.5, 0.6, 0.8\}$, and use $(\alpha, \beta) = (0.6, 0.4)$ for forecasting and classification, and $(\alpha, \beta) = (0.2, 0.8)$ for imputation and anomaly detection. For tokenization, we fix the patch size and stride to $P = S = 8$.

Table 2: Long-term forecasting results with lookback length $T = 96$ and prediction length $S \in \{96, 192, 336, 720\}$. Lower MSE or MAE is better.

Models	SSD + DALA		SSM-based						Transformer-based models						MLP-based models						TCN-based models																	
	DeMa (Ours)		Affirm			S-Mamba			CMamba			SAMBA			iTTransformer			Crossformer			PatchTST			TimeMixer			RLinear			DLinear			ModernTCN			TimesNet		
	Metric	MSE	MAE	MSE	MAE	MSE	MAE	MSE	MAE	MSE	MAE	MSE	MAE	MSE	MAE	MSE	MAE	MSE	MAE	MSE	MAE	MSE	MAE	MSE	MAE	MSE	MAE	MSE	MAE	MSE	MAE	MSE	MAE					
Electricity	96	0.137	0.201	0.148	0.231	0.139	0.235	0.141	0.231	0.146	0.244	0.148	0.240	0.219	0.314	0.181	0.270	0.153	0.247	0.201	0.281	0.197	0.282	0.171	0.269	0.168	0.272											
	192	0.155	0.220	0.158	0.237	0.159	0.255	0.157	0.245	0.162	0.243	0.231	0.322	0.188	0.274	0.166	0.256	0.201	0.283	0.196	0.285	0.193	0.287	0.184	0.289													
	336	0.172	0.252	0.177	0.268	0.176	0.272	0.175	0.265	0.177	0.274	0.178	0.269	0.244	0.307	0.204	0.293	0.185	0.277	0.215	0.298	0.209	0.301	0.205	0.297	0.199	0.300											
	720	0.195	0.271	0.206	0.295	0.204	0.298	0.203	0.289	0.202	0.297	0.225	0.317	0.280	0.363	0.246	0.324	0.225	0.310	0.257	0.331	0.245	0.333	0.217	0.276	0.220	0.320											
	Avg	0.165	0.236	0.172	0.258	0.170	0.265	0.169	0.258	0.172	0.268	0.178	0.270	0.244	0.334	0.205	0.290	0.182	0.272	0.219	0.298	0.212	0.300	0.197	0.282	0.192	0.295											
ETTh1h	96	0.359	0.372	0.375	0.396	0.386	0.405	0.372	0.386	0.376	0.400	0.386	0.405	0.423	0.448	0.414	0.419	0.375	0.400	0.386	0.395	0.386	0.400	0.371	0.389	0.384	0.402											
	192	0.413	0.415	0.421	0.428	0.443	0.437	0.416	0.432	0.429	0.441	0.436	0.471	0.474	0.460	0.445	0.429	0.421	0.437	0.424	0.437	0.432	0.423	0.439	0.436	0.429												
	336	0.451	0.438	0.438	0.472	0.489	0.468	0.466	0.438	0.477	0.437	0.487	0.458	0.570	0.546	0.501	0.466	0.484	0.458	0.457	0.446	0.481	0.459	0.486	0.445	0.491	0.469											
	720	0.467	0.452	0.494	0.469	0.502	0.489	0.470	0.461	0.503	0.491	0.652	0.504	0.488	0.498	0.482	0.481	0.470	0.519	0.516	0.501	0.486	0.521	0.500														
	Avg	0.423	0.419	0.434	0.441	0.455	0.450	0.433	0.425	0.443	0.432	0.454	0.447	0.529	0.522	0.469	0.454	0.447	0.440	0.446	0.434	0.456	0.452	0.445	0.440	0.458	0.450											
ETTh2	96	0.285	0.335	0.300	0.344	0.296	0.348	0.281	0.329	0.288	0.340	0.297	0.349	0.745	0.584	0.302	0.348	0.289	0.341	0.288	0.338	0.333	0.387	0.321	0.348	0.340	0.374											
	192	0.365	0.383	0.382	0.397	0.376	0.396	0.361	0.381	0.373	0.390	0.380	0.400	0.877	0.656	0.388	0.400	0.372	0.372	0.392	0.380	0.389	0.357	0.377	0.374	0.387												
	336	0.388	0.402	0.418	0.427	0.408	0.413	0.390	0.389	0.405	0.426	0.420	0.532	0.515	0.399	0.410	0.390	0.404	0.424	0.415	0.413	0.413	0.402	0.410	0.410	0.411												
	720	0.418	0.446	0.427	0.467	0.426	0.444	0.419	0.419	0.412	0.435	0.427	0.445	1.104	0.763	0.431	0.446	0.412	0.434	0.420	0.440	0.403	0.457	0.431	0.440	0.462	0.468											
	Avg	0.370	0.396	0.381	0.413	0.381	0.405	0.368	0.391	0.363	0.392	0.383	0.407	0.402	0.364	0.395	0.374	0.398	0.359	0.351	0.381	0.404	0.414	0.427														
ETTm1	96	0.292	0.343	0.337	0.369	0.333	0.368	0.308	0.338	0.334	0.357	0.337	0.368	0.404	0.426	0.329	0.367	0.320	0.357	0.355	0.376	0.345	0.372	0.327	0.365	0.338	0.375											
	192	0.365	0.387	0.372	0.382	0.376	0.390	0.359	0.364	0.360	0.383	0.377	0.391	0.450	0.451	0.367	0.385	0.361	0.381	0.391	0.392	0.380	0.389	0.357	0.377	0.374	0.387											
	336	0.388	0.402	0.418	0.427	0.408	0.413	0.390	0.389	0.405	0.426	0.420	0.532	0.515	0.399	0.410	0.390	0.404	0.424	0.415	0.413	0.413	0.402	0.410	0.410	0.411												
	720	0.422	0.423	0.472	0.450	0.475	0.448	0.447	0.425	0.448	0.440	0.491	0.459	0.666	0.589	0.454	0.439	0.454	0.441	0.487	0.450	0.474	0.453	0.458	0.453	0.478	0.450											
	Avg	0.367	0.389	0.400	0.407	0.398	0.405	0.376	0.379	0.378	0.394	0.407	0.410	0.513	0.496	0.387	0.400	0.381	0.395	0.414	0.407	0.403	0.407	0.386	0.401	0.400	0.406											
ETTm2	96	0.169	0.256	0.179	0.264	0.179	0.263	0.171	0.248	0.172	0.259	0.180	0.264	0.287	0.366	0.175	0.259	0.175	0.258	0.182	0.265	0.193	0.292	0.171	0.262	0.187	0.267											
	192	0.230	0.290	0.251	0.308	0.250	0.309	0.235	0.292	0.238	0.301	0.250	0.309	0.414	0.492	0.241	0.302	0.237	0.294	0.246	0.304	0.284	0.362	0.227	0.286	0.249	0.309											
	336	0.282	0.327	0.317	0.350	0.312	0.349	0.296	0.334	0.300	0.340	0.311	0.348	0.597	0.542	0.305	0.343	0.298	0.340	0.307	0.342	0.369	0.427	0.325	0.335	0.321	0.351											
	720	0.398	0.397	0.405	0.411	0.406	0.392	0.391	0.412	0.412	0.407	0.401	0.406	0.592	0.510	0.394	0.407	0.398	0.402	0.400	0.391	0.396	0.407	0.398	0.558	0.522	0.388	0.405	0.408	0.403								
	Avg	0.270	0.318	0.288	0.331	0.288	0.332	0.273	0.316	0.276	0.322	0.288	0.332	0.575	0.610	0.281	0.326	0.275	0.323	0.284	0.327	0.350	0.401	0.278	0.322	0.291	0.333											
Exchange	96	0.075	0.186	0.088	0.202	0.086	0.207	0.083	0.202	0.086	0.206	0.085	0.205	0.094	0.218	0.093	0.217	0.088	0.218	0.089	0.202	0.107	0.234															
	192	0.152	0.283	0.178	0.298	0.182	0.304	0.178	0.306	0.176	0.298	0.177	0.299	0.184	0.308	0.207	0.307	0.176	0.298	0.175	0.290	0.187	0.315	0.187	0.314	0.226	0.344											
	336	0.301	0.395	0.351	0.412	0.332	0.418	0.330	0.417	0.327	0.413	0.331	0.417	0.268	0.883	0.301	0.397	0.349	0.431	0.351	0.432	0.313	0.427	0.328	0.428	0.367	0.448											
	720	0.841	0.682	0.887	0.716	0.867	0.703	0.843	0.693	0.839	0.689	0.847	0.691	1.767	1.068	0.901	0.714	0.852	0.698	0.886	0.714	0.839	0.695	0.925	0.721	0.964	0.746											
	Avg	0.342	0.387	0.376	0.407	0.367	0.408	0.359	0.405																													

and modeling temporal and variate dependencies is more effective for long-horizon forecasting than relying solely on global attention. It also consistently surpasses Mamba variants and non-attention models—for example, on Traffic (Avg), DeMa reduces MSE by 10.1% over the strongest Mamba baseline (S-Mamba, 0.414) and achieves clear gains over representative MLP and TCN baselines (TimeMixer, 0.484; ModernTCN, 0.546). These improvements stem from DeMa’s comprehensive dependency modeling: Mamba-SSD efficiently captures cross-time dependencies via parallel selective state-space computation, while Mamba-DALA strengthens cross-variate interaction modeling. Their synergy enables DeMa to jointly exploit long-range temporal structures and inter-series correlations, yielding consistently top performance in long-term forecasting.

Table 3: Short-term forecasting results with lookback length $T = 96$ and prediction length $S \in \{12, 24, 48\}$. Lower MSE or MAE is better.

Models	SSD + DALA		SSM-based				Transformer-based models			MLP-based models			TCN-based models		
	DeMa (Ours)		Affirm [56]	S-Mamba [57]	CMamba [58]	SAMBA [59]	iTransformer [11]	Crossformer [24]	PatchTST [8]	TimeMixer [19]	RLinear [60]	DLinear [18]	ModernTCN [17]	TimesNet [12]	
	Metric	MSE	MAE	MSE	MAE	MSE	MAE	MSE	MAE	MSE	MAE	MSE	MAE	MSE	MAE
PEMS03	12	0.050	0.146	0.091 0.200	0.065 0.169	0.068 0.172	0.066 0.182	0.071 0.174	0.090 0.203	0.099 0.216	0.073 0.181	0.126 0.236	0.122 0.243	0.072 0.186	0.085 0.192
	24	0.063	0.172	0.104 0.228	0.087 0.196	0.079 0.201	0.075 0.203	0.093 0.201	0.121 0.240	0.142 0.259	0.091 0.232	0.246 0.334	0.201 0.317	0.095 0.217	0.118 0.223
	48	0.093	0.204	0.199 0.281	0.133 0.243	0.132 0.239	0.147 0.255	0.125 0.236	0.202 0.317	0.211 0.319	0.138 0.244	0.551 0.529	0.333 0.425	0.136 0.249	0.155 0.260
	Avg	0.069	0.174	0.131 0.236	0.095 0.203	0.093	0.204	0.096 0.213	0.096 0.204	0.138 0.253	0.151 0.265	0.101 0.219	0.308 0.366	0.219 0.328	0.101 0.217
	1 st Count	16	16	0 0	0 0	0 0	0 0	0 0	0 0	0 0	0 0	0 0	0 0	0 0	0 0
PEMS04	12	0.061	0.168	0.092 0.201	0.076 0.180	0.079 0.199	0.073 0.172	0.078 0.183	0.098 0.218	0.105 0.224	0.082 0.201	0.138 0.252	0.148 0.272	0.082 0.192	0.087 0.195
	24	0.062	0.172	0.119 0.256	0.084 0.193	0.093 0.228	0.086 0.185	0.095 0.205	0.131 0.256	0.153 0.275	0.102 0.222	0.258 0.348	0.224 0.340	0.093 0.209	0.103 0.215
	48	0.087	0.193	0.187 0.283	0.115 0.224	0.156 0.266	0.092 0.209	0.120 0.233	0.205 0.326	0.229 0.339	0.157 0.289	0.572 0.544	0.355 0.437	0.123 0.227	0.136 0.250
	Avg	0.070	0.178	0.133 0.247	0.092 0.199	0.109 0.231	0.083 0.189	0.098 0.207	0.145 0.267	0.162 0.279	0.114 0.238	0.323 0.381	0.242 0.350	0.099 0.209	0.109 0.220
	1 st Count	16	16	0 0	0 0	0 0	0 0	0 0	0 0	0 0	0 0	0 0	0 0	0 0	0 0
PEMS07	12	0.059	0.147	0.083 0.192	0.063 0.159	0.069 0.172	0.067 0.177	0.067 0.165	0.094 0.200	0.095 0.207	0.078 0.181	0.118 0.235	0.115 0.242	0.073 0.175	0.082 0.181
	24	0.069	0.162	0.128 0.227	0.081 0.183	0.092 0.194	0.094 0.211	0.088 0.190	0.139 0.247	0.150 0.262	0.108 0.239	0.242 0.341	0.210 0.329	0.095 0.193	0.101 0.204
	48	0.079	0.174	0.205 0.299	0.093 0.192	0.137 0.255	0.122 0.236	0.110 0.215	0.311 0.369	0.253 0.340	0.167 0.292	0.562 0.541	0.398 0.458	0.116 0.221	0.134 0.238
	Avg	0.069	0.161	0.139 0.240	0.079 0.178	0.099 0.207	0.094 0.208	0.088 0.190	0.181 0.272	0.166 0.270	0.118 0.237	0.307 0.372	0.241 0.343	0.095 0.196	0.106 0.208
	1 st Count	16	16	0 0	0 0	0 0	0 0	0 0	0 0	0 0	0 0	0 0	0 0	0 0	0 0
PEMS08	12	0.052	0.158	0.141 0.192	0.076 0.178	0.082 0.199	0.080 0.191	0.079 0.182	0.165 0.214	0.168 0.232	0.144 0.216	0.196 0.247	0.154 0.276	0.082 0.181	0.112 0.212
	24	0.091	0.183	0.183 0.299	0.104 0.209	0.134 0.238	0.116 0.221	0.115 0.219	0.215 0.260	0.224 0.281	0.181 0.272	0.249 0.343	0.248 0.353	0.129 0.227	0.141 0.238
	48	0.149	0.206	0.237 0.307	0.167 0.228	0.200 0.255	0.199 0.241	0.186 0.235	0.315 0.355	0.321 0.354	0.259 0.323	0.569 0.544	0.440 0.470	0.183 0.231	0.198 0.283
	Avg	0.097	0.182	0.187 0.266	0.116 0.205	0.139 0.231	0.132 0.218	0.127 0.212	0.232 0.276	0.238 0.289	0.195 0.264	0.317 0.378	0.281 0.366	0.131 0.213	0.150 0.244
	1 st Count	16	16	0 0	0 0	0 0	0 0	0 0	0 0	0 0	0 0	0 0	0 0	0 0	0 0

4.3.2 Short-term Forecasting Results

We evaluate short-term forecasting on four PEMS traffic benchmarks, where accurate prediction is challenging due to intricate spatiotemporal dependencies among sensors and strong inter-series interactions that drive citywide traffic dynamics. Table 3 summarizes the results under a fixed lookback length $T = 96$ and prediction horizons $S \in \{12, 24, 48\}$. Overall, DeMa achieves the best performance in all 16 settings (both MSE and MAE), demonstrating its strong effectiveness for short-term forecasting. In terms of averaged MSE, DeMa improves over the strongest competitor by a clear margin, reducing errors by 25.8% on PEMS03, 15.7% on PEMS04, 12.7% on PEMS07, and 16.4% on PEMS08. Notably, variate-independent architectures exhibit pronounced performance degradation on these datasets. For example, PatchTST, which largely models each variate independently, is consistently inferior to DeMa across all horizons; a similar trend is observed for MLP-based methods, whose channel-independent mixing fails to capture dynamic cross-sensor interactions. We attribute the consistent gains of DeMa to its explicit and effective cross-variate modeling: Mamba-DALA strengthens cross-variate interactions, including delay-aware dependencies among traffic sensors, and complements the cross-time temporal modeling of Mamba-SSD. Their synergy enables DeMa to jointly exploit temporal dynamics and delay-aware inter-sensor dependencies, resulting in substantially improved short-term forecasting performance on the PEMS benchmarks.

4.3.3 Imputation Results

Time series imputation aims to recover missing values from partially observed series, which is crucial in real-world scenarios where data acquisition is imperfect due to sensor malfunctions or unexpected transmission glitches. As reported in Table 4, DeMa consistently achieves the best performance across all datasets and masking ratios, surpassing both Transformer-based and SSM-based competitors by clear margins. A notable trend is that the advantage of DeMa becomes more pronounced as the missing rate increases, where accurate recovery increasingly relies on fine-grained modeling of local fluctuations and precise temporal alignment between observed contexts and missing entries. For instance, on ETTh1 with 50% masking, DeMa attains a low error of 0.064/0.159,

whereas Transformer baselines (e.g., PatchTST: 0.173/0.271; iTransformer: 0.142/0.286) and SSM-based methods (e.g., S-Mamba: 0.142/0.281) degrade substantially, indicating limited capability in capturing the local variations required for reliable completion. These results suggest that imputation is not merely a global dependency modeling problem, but a fine-grained completion task that hinges on (i) local context continuity around missing positions and (ii) accurate relative lag relations between correlated variates. Concretely, Mamba-SSD provides efficient temporal context aggregation to supply informative local cues, while Mamba-DALA enables delay-aware cross-variate interactions so that observed variates can contribute aligned evidence for reconstructing missing values. Together, their synergy facilitates more precise recovery of local dynamics and inter-series signals, leading to consistently superior imputation accuracy.

Table 4: Imputation results on 96-length input windows with random masking ratios {12.5%, 25%, 37.5%, 50%}. Lower MSE or MAE is better.

Models	SSD + DALA				SSM-based				Transformer-based models				MLP-based models				TCN-based models											
	DeMa (Ours)		Affirm [56]		S-Mamba [57]		CMamba [58]		SAMBA [59]		iTransformer [11]		Crossformer [24]		PatchTST [8]		TimeMixer [19]		RLinear [60]		DLinear [18]		ModemTCN [17]		TimesNet [12]			
	Metric	MSE	MAE	MSE	MAE	MSE	MAE	MSE	MAE	MSE	MAE	MSE	MAE	MSE	MAE	MSE	MAE	MSE	MAE	MSE	MAE	MSE	MAE	MSE	MAE			
ETTh1	12.5%	0.032	0.122	0.133	0.242	0.112	0.221	0.101	0.211	0.116	0.256	0.111	0.223	0.099	0.218	0.094	0.199	0.127	0.232	0.099	0.206	0.151	0.267	0.035	0.128	0.057	0.159	
	25%	0.042	0.131	0.142	0.249	0.131	0.242	0.127	0.238	0.138	0.247	0.129	0.257	0.125	0.243	0.119	0.225	0.135	0.267	0.123	0.229	0.180	0.292	0.042	0.140	0.069	0.178	
	37.5%	0.052	0.137	0.151	0.276	0.140	0.251	0.139	0.244	0.142	0.251	0.133	0.263	0.146	0.263	0.145	0.248	0.149	0.279	0.153	0.253	0.215	0.318	0.054	0.157	0.084	0.196	
	50%	0.064	0.159	0.164	0.292	0.142	0.281	0.142	0.279	0.146	0.288	0.142	0.286	0.158	0.281	0.173	0.271	0.151	0.291	0.188	0.278	0.257	0.347	0.067	0.174	0.102	0.215	
Avg		0.048	0.137	0.147	0.265	0.131	0.249	0.127	0.243	0.136	0.261	0.129	0.257	0.132	0.251	0.133	0.236	0.141	0.267	0.141	0.242	0.201	0.306	0.050	0.150	0.078	0.187	
ETTh2	12.5%	0.035	0.120	0.099	0.183	0.071	0.172	0.067	0.165	0.073	0.174	0.056	0.152	0.109	0.220	0.057	0.150	0.044	0.133	0.057	0.152	0.100	0.216	0.037	0.121	0.040	0.130	
	25%	0.038	0.126	0.103	0.190	0.077	0.176	0.072	0.167	0.082	0.181	0.061	0.162	0.110	0.229	0.062	0.158	0.051	0.132	0.062	0.160	0.127	0.247	0.040	0.127	0.046	0.141	
	37.5%	0.041	0.138	0.118	0.199	0.088	0.188	0.078	0.179	0.088	0.190	0.076	0.169	0.129	0.246	0.068	0.168	0.062	0.191	0.068	0.168	0.158	0.276	0.043	0.134	0.052	0.151	
	50%	0.045	0.142	0.122	0.217	0.085	0.203	0.083	0.191	0.090	0.208	0.079	0.177	0.148	0.265	0.076	0.179	0.083	0.200	0.076	0.179	0.183	0.299	0.048	0.143	0.060	0.162	
Avg		0.040	0.132	0.111	0.197	0.079	0.185	0.075	0.176	0.083	0.188	0.068	0.165	0.122	0.240	0.066	0.164	0.060	0.159	0.061	0.165	0.142	0.259	0.042	0.131	0.049	0.146	
ETTm1	12.5%	0.015	0.081	0.061	0.152	0.047	0.131	0.052	0.135	0.055	0.123	0.059	0.128	0.037	0.137	0.041	0.128	0.042	0.113	0.047	0.137	0.058	0.162	0.015	0.082	0.019	0.092	
	25%	0.020	0.083	0.073	0.177	0.065	0.169	0.063	0.157	0.068	0.163	0.062	0.142	0.038	0.141	0.043	0.130	0.055	0.135	0.061	0.157	0.080	0.193	0.018	0.088	0.023	0.101	
	37.5%	0.023	0.093	0.079	0.196	0.077	0.188	0.072	0.182	0.083	0.191	0.075	0.203	0.044	0.142	0.044	0.133	0.068	0.197	0.077	0.175	0.103	0.219	0.021	0.095	0.029	0.111	
	50%	0.024	0.100	0.099	0.216	0.091	0.201	0.091	0.199	0.088	0.202	0.096	0.215	0.047	0.152	0.050	0.142	0.083	0.202	0.098	0.195	0.132	0.248	0.026	0.105	0.036	0.124	
Avg		0.021	0.090	0.078	0.185	0.070	0.169	0.074	0.170	0.073	0.172	0.041	0.143	0.045	0.133	0.062	0.162	0.070	0.166	0.093	0.206	0.020	0.093	0.027	0.107			
ETTm2	12.5%	0.016	0.074	0.037	0.139	0.029	0.122	0.035	0.117	0.033	0.108	0.030	0.094	0.044	0.148	0.025	0.092	0.031	0.103	0.026	0.093	0.062	0.166	0.017	0.076	0.018	0.080	
	25%	0.021	0.079	0.044	0.142	0.035	0.129	0.042	0.128	0.040	0.112	0.031	0.096	0.047	0.151	0.027	0.095	0.040	0.108	0.030	0.103	0.085	0.196	0.018	0.080	0.020	0.085	
	37.5%	0.023	0.095	0.059	0.155	0.048	0.132	0.053	0.137	0.047	0.137	0.039	0.107	0.045	0.145	0.029	0.099	0.044	0.117	0.034	0.113	0.106	0.222	0.020	0.084	0.023	0.091	
	50%	0.025	0.099	0.066	0.161	0.051	0.145	0.063	0.166	0.059	0.159	0.041	0.129	0.047	0.150	0.032	0.109	0.047	0.139	0.039	0.123	0.131	0.247	0.022	0.090	0.026	0.098	
Avg		0.021	0.087	0.052	0.149	0.040	0.132	0.047	0.137	0.045	0.129	0.035	0.107	0.046	0.149	0.028	0.098	0.041	0.117	0.032	0.108	0.096	0.208	0.019	0.082	0.022	0.088	
Electricity	12.5%	0.052	0.142	0.077	0.189	0.063	0.171	0.072	0.189	0.077	0.190	0.064	0.172	0.068	0.181	0.073	0.188	0.094	0.205	0.079	0.199	0.092	0.214	0.059	0.171	0.085	0.202	
	25%	0.067	0.161	0.081	0.192	0.072	0.187	0.088	0.199	0.081	0.218	0.073	0.188	0.078	0.198	0.082	0.200	0.103	0.213	0.082	0.233	0.118	0.247	0.071	0.188	0.089	0.206	
	37.5%	0.076	0.171	0.089	0.219	0.177	0.193	0.092	0.208	0.099	0.223	0.087	0.200	0.087	0.208	0.097	0.217	0.116	0.231	0.131	0.262	0.144	0.276	0.077	0.190	0.094	0.213	
	50%	0.077	0.182	0.095	0.226	0.089	0.204	0.118	0.213	0.115	0.237	0.091	0.205	0.098	0.212	0.110	0.232	0.132	0.255	0.160	0.291	0.175	0.305	0.085	0.200	0.100	0.221	
Avg		0.068	0.164	0.086	0.207	0.079	0.189	0.093	0.202	0.093	0.217	0.079	0.191	0.083	0.199	0.091	0.209	0.111	0.226	0.119	0.246	0.132	0.260	0.073	0.187	0.092	0.210	
Weather	12.5%	0.021	0.035	0.034	0.041	0.025	0.039	0.031	0.045	0.029	0.051	0.027	0.041	0.034	0.092	0.029	0.049	0.032	0.043	0.026	0.048	0.039	0.084	0.023	0.038	0.025	0.045	
	25%	0.023	0.039	0.039	0.042	0.025	0.036	0.046	0.037	0.059	0.033	0.055	0.031	0.047	0.035	0.088	0.031	0.053	0.035	0.049	0.032	0.055	0.048	0.103	0.025	0.041	0.029	0.052
	37.5%	0.025	0.041	0.042	0.046	0.033	0.053	0.042	0.063	0.037	0.062	0.033	0.059	0.035	0.088	0.034	0.058	0.038	0.062	0.037	0.067	0.057	0.117	0.027	0.046	0.031	0.057	
	50%	0.029	0.049	0.050	0.069	0.035	0.059	0.049	0.071	0.046	0.067	0.036	0.062	0.038	0.092	0.039	0.066	0.044	0.060	0.040	0.067	0.066	0.134	0.031	0.051	0.034	0.062	
Avg		0.025	0.041	0.041	0.057	0.030	0.049	0.040	0.060	0.036	0.059	0.032	0.052	0.036	0.090	0.033	0.057	0.037	0.054	0.034	0.058	0.052	0.110	0.027	0.044	0.030	0.054	
1 st Count	23	25	0	0	0	0	0	0	0	0	0	0	0	0	0	0	0	0	0	0	0	0	0	2	5	0	0	

4.4 Classification Results

Time series classification aims to assign a semantic label to a multivariate series by recognizing both global patterns and discriminative local cues. We evaluate on ten multivariate datasets from the UEA Time Series Archive [62], and report the average classification accuracy of each method across the ten benchmarks. As shown in Figure 3(a), DeMa achieves the highest average accuracy of 76.3%, consistently outperforming strong baselines from all major families, including ModernTCN (74.2%), TimesNet (73.6%), Crossformer (73.2%), and TimeMixer (73.1%). A key observation is that TCN-based methods achieve competitive performance on classification. This is because temporal convolutions provide a strong inductive bias for extracting discriminative local motifs, e.g., shape-like patterns, that are often sufficient to determine class labels. With hierarchical convolutions, TCNs can further aggregate multi-scale evidence while remaining robust to small phase shifts and noise through parameter sharing and localized receptive fields, making them particularly effective for semantic recognition. In contrast, MLP-based approaches remain inferior (e.g., DLinear: 67.5%, RLinear: 70.0%), since their predominantly linear mixing is less capable of building high-level semantic features and modeling complex inter-series interactions. The superior performance of DeMa stems from its fine-grained and hierarchical dependency encoding: stacking DuoMNet blocks progressively aggregates multi-scale temporal evidence, while the dual-path design explicitly captures both temporal variations and cross-variate cues. In particular, Mamba-SSD strengthens long-range temporal structure modeling, and Mamba-DALA enhances cross-variate interactions, enabling DeMa

to form more informative and semantically aligned representations for classification beyond purely convolutional local feature extraction.

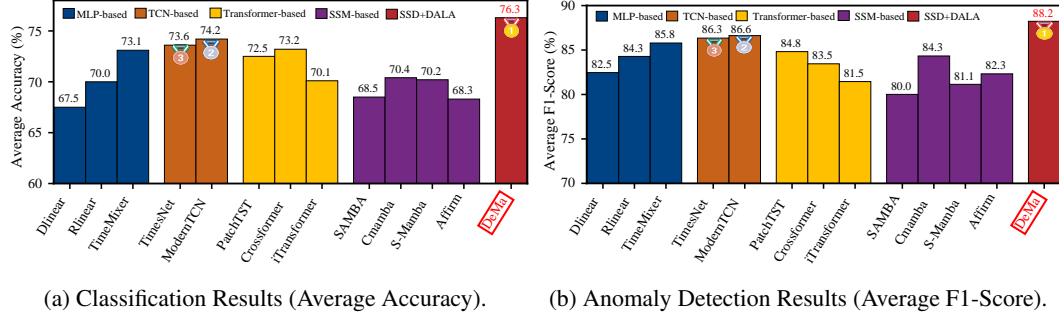


Figure 3: Performance comparison on classification and anomaly detection tasks. Results are averaged over multiple datasets; higher is better.

4.4.1 Anomaly Detection Results

Anomaly detection aims to identify rare and abnormal patterns in time series, which often correspond to faults, critical events, or outliers requiring timely intervention. Following prior work [33], we evaluate on five widely used anomaly detection benchmarks and report the average F1-score across datasets. For fair comparison, we adopt reconstruction error [12] as the anomaly criterion for all methods. As shown in Figure 3(b), DeMa achieves the best average F1-score of 88.2%, outperforming strong competitors such as ModernTCN (86.6%) and TimesNet (86.3%). This gain highlights the advantage of our fine-grained modeling. The proposed SSD+DALA design jointly strengthens (i) local temporal continuity and long-range temporal context via Mamba-SSD, and (ii) delay-aware cross-variate interactions via Mamba-DALA, enabling more faithful reconstruction of normal dynamics. As a result, abnormal deviations yield sharper and more separable reconstruction residuals, leading to improved detection accuracy. In contrast, iTransformer [11] and S-Mamba [57] perform notably worse, likely because their series-wise global similarity modeling by attention can be dominated by prevalent normal patterns; consequently, the subtle abnormal segments are more easily diluted when aggregating pairwise correlations, leading to inferior detection. Finally, we observe that methods benefiting from explicit decomposition cues (e.g., TimesNet and DeMa) tend to achieve stronger overall detection performance, underscoring the importance of separating stable periodic structures from irregular fluctuations so that violations of normal regularities become more detectable.

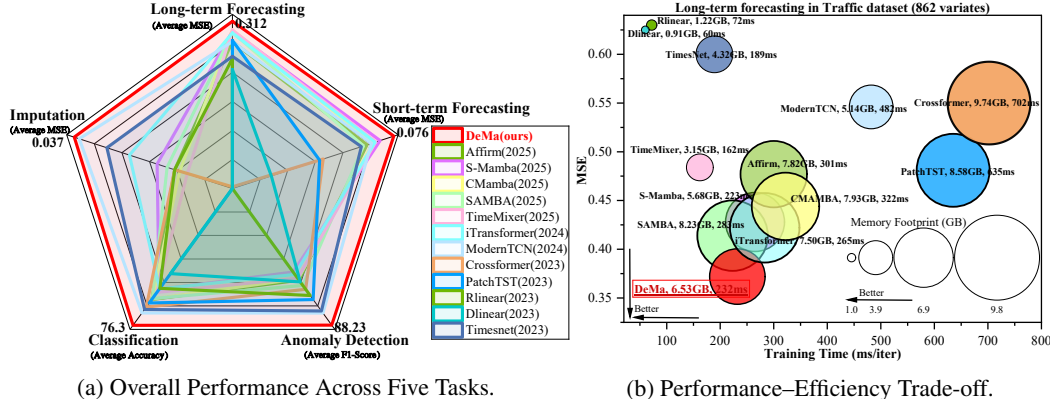
4.5 Performance-Efficiency Trade-off (RQ2)

Figure 4 summarizes the overall effectiveness and efficiency of DeMa. Figure 4(a) provides an overall comparison of baselines across five representative time-series tasks. Overall, DeMa achieves consistently strong results on all tasks, demonstrating robust task generality rather than tuning to a single forecasting setting. Figure 4(b) further evaluates the accuracy-efficiency trade-off on a large-scale traffic dataset with 862 variates under long-term forecasting, where the y-axis denotes MSE, the x-axis indicates training time, and the bubble size reflects GPU memory footprint. As shown, DeMa attains the lowest MSE (0.372) with moderate training time (232 ms/iter) and manageable memory usage (6.53 GB), offering a favorable balance between accuracy and computational cost. These results suggest that DeMa is a practical and scalable solution for large-scale multivariate time-series analysis.

DeMa exhibits clear efficiency advantages over Transformer-based baselines while remaining more accurate, benefiting from the linear-time state-space backbone. For instance, Crossformer and PatchTST require substantially higher training time and memory footprint (e.g., 702 ms/iter and 9.74 GB for Crossformer), yet still yield higher MSE than DeMa in Figure 4(b). Moreover, DeMa consistently outperforms TCN-based models in the multi-task comparison (Figure 4(a)). While TCNs are efficient and effective at capturing local motifs, their limited receptive field and forecasting-oriented inductive bias may restrict transferability to tasks that require long-range aggregation. In contrast, DeMa learns more transferable representations by jointly encoding long-range temporal dynamics and delay-aware inter-series interactions. Finally, DeMa improves the accuracy-efficiency

trade-off over recent Mamba variants. As shown in Figure 4(b), DeMa is faster and lighter than Affirm and CMamba (e.g., 232 ms/iter and 6.53 GB for DeMa versus 301 ms/iter and 7.82 GB for Affirm, and 322 ms/iter and 7.93 GB for CMamba), while achieving lower MSE.

In summary, DeMa combines state-of-the-art accuracy with practical training speed and memory cost, making it a strong candidate for scalable and general time-series analysis.



(a) Overall Performance Across Five Tasks.

(b) Performance-Efficiency Trade-off.

Figure 4: Model performance comparison (left) and efficiency comparison (right). DeMa achieves consistent state-of-the-art performance across five mainstream time-series tasks. Meanwhile, DeMa attains the lowest mean squared error while maintaining shorter training time and a smaller memory footprint.

4.6 Scalability vs. Input Length (RQ3)

Semantic information in time series are often formed by aggregating evidence over long horizons rather than isolated timestamps. Although longer lookback windows provide richer context, they also place stricter demands on training efficiency and GPU memory. To evaluate scalability with respect to the input length, Figure 5 reports the per-iteration running time and GPU memory footprint of DeMa and representative Transformer-based baselines on ETTh1. We increase the lookback length from $\{384, 768, 1536, 3072\}$ while fixing the embedding dimension to $d = 256$ for a fair comparison. As shown, DeMa consistently achieves the lowest running time and memory usage across all lengths, and its growth remains close to linear as the series length increases. By contrast, Transformer-based methods (e.g., Transformer, PatchTST and Crossformer) exhibit rapidly increasing computation and memory overhead with longer inputs, which substantially limits their practicality in long-horizon settings. Notably, iTransformer is more efficient than token-wise Transformers because it computes series-wise attention, avoiding the quadratic growth with respect to the token length; nevertheless, it is still consistently slower and more memory-intensive than DeMa at large input lengths.

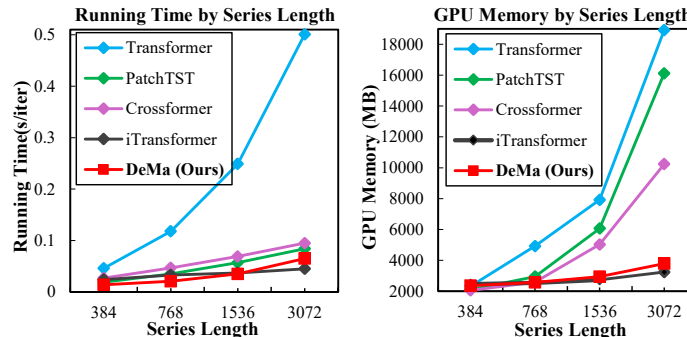


Figure 5: Efficiency analysis of GPU memory and running time in a long-term lookback-window scenario. Our proposed DeMa scales linearly with the series length, whereas the vanilla Transformer exhibits quadratic complexity with respect to the series length.

These observations align with our complexity analysis in Figure 1(b). Leveraging the parallelizable Mamba-SSD and Mamba-DALA blocks, DeMa scales linearly with the token length, with time complexity $\mathcal{O}(2NLd^2)$, where N is the number of variates, L is the number of tokens after tokenization, and d is the embedding dimension. In typical long-horizon MTS scenarios, $L, N \gg d$, making DeMa a more scalable backbone for long-horizon and large-scale multivariate time-series modeling.

4.7 Ablation Study (RQ4)

To quantify the contribution of each key component in DeMa, including the Adaptive Fourier Filter, Mamba-SSD, and Mamba-DALA, we conduct ablation studies on Traffic (long-term forecasting) and PEMS04 (short-term forecasting). As reported in Table 5, we consider two types of ablations: *replacement* (*Repl.*), which substitutes a target module with an alternative design, and *removal* (*w/o*), which disables the module entirely. Overall, each component consistently improves forecasting accuracy, and the full model yields the best performance on both datasets.

Table 5: Ablation study of DeMa.

No.	Design	Decomp.	Variate	Temporal	Traffic		PEMS04	
					MSE	MAE	MSE	MAE
1	DeMa	Fourier	Mamba-DALA	Mamba-SSD	0.382	0.247	0.061	0.168
2		Fourier	Mamba-SSD	Mamba-DALA	0.416	0.297	0.093	0.204
3	Repl.	Fourier	Mamba-DALA	Mamba-DALA	0.507	0.314	0.126	0.257
4		Fourier	Mamba-SSD	Mamba-SSD	0.412	0.295	0.087	0.192
5		w/o	Mamba-DALA	Mamba-SSD	0.415	0.279	0.097	0.215
6	w/o	w/o	w/o	Mamba-SSD	0.539	0.317	0.142	0.267
7		w/o	Mamba-DALA	w/o	0.597	0.383	0.225	0.337

- **Adaptive Fourier Filter.** Comparing Rows 1 and 5, removing the decomposition module causes clear degradation on both datasets (Traffic MSE: $0.382 \rightarrow 0.415$; PEMS04 MSE: $0.061 \rightarrow 0.097$). This verifies that the Adaptive Fourier Filter provides a beneficial decomposition prior by separating slowly varying structures (e.g., trend and seasonality) from short-term fluctuations, thereby reducing spectral interference and facilitating more reliable dependency modeling in both the temporal and variate paths, consistent with decomposition-based forecasting literature [40, 22].
- **Mamba-SSD for temporal modeling.** Rows 2–3 replace the temporal Mamba-SSD with attention-style alternatives, leading to substantial performance drops (e.g., Row 3: Traffic MSE $0.382 \rightarrow 0.507$, a 32.7% increase). This indicates that Mamba-SSD is critical for efficiently capturing long-range temporal dynamics. Moreover, removing the temporal path entirely (Row 7) results in the largest degradation (Traffic MSE $0.382 \rightarrow 0.597$, +56.3%; PEMS04 MSE $0.061 \rightarrow 0.225$), confirming that strong cross-time modeling is indispensable for accurate forecasting.
- **Mamba-DALA for cross-variate interaction modeling.** Rows 4 and 6 highlight the necessity of Mamba-DALA for modeling cross-variate dependencies. Replacing Mamba-DALA with a temporal-style Mamba-SSD interaction (Row 4) already hurts performance (Traffic MSE $0.382 \rightarrow 0.412$; PEMS04 MSE $0.061 \rightarrow 0.087$), suggesting that directly reusing temporal mechanisms is insufficient for variate interactions. More importantly, removing Mamba-DALA (Row 6) causes a pronounced drop (Traffic MSE $0.382 \rightarrow 0.539$, +41.1%; PEMS04 MSE $0.061 \rightarrow 0.142$), verifying that delay-aware cross-variate modeling provides critical complementary cues beyond temporal dynamics.

4.8 Hyperparameter Sensitivity Analysis (RQ5)

In DeMa, we adopt a weighted fusion layer to combine the temporal-path representation and the variate-path representation, controlled by the fusion weights α and β in Eq. (28). To examine the sensitivity of this fusion trade-off, we perform a grid search over $\alpha, \beta \in \{0.2, 0.4, 0.5, 0.6, 0.8\}$ on forecasting and imputation on Weather [22], classification on Heartbeat [55], and anomaly detection on MSL [52]. The results are summarized in Figure 6(a)–(d), where higher is better for Accuracy, F1-score, and $1/\text{MAE}$.

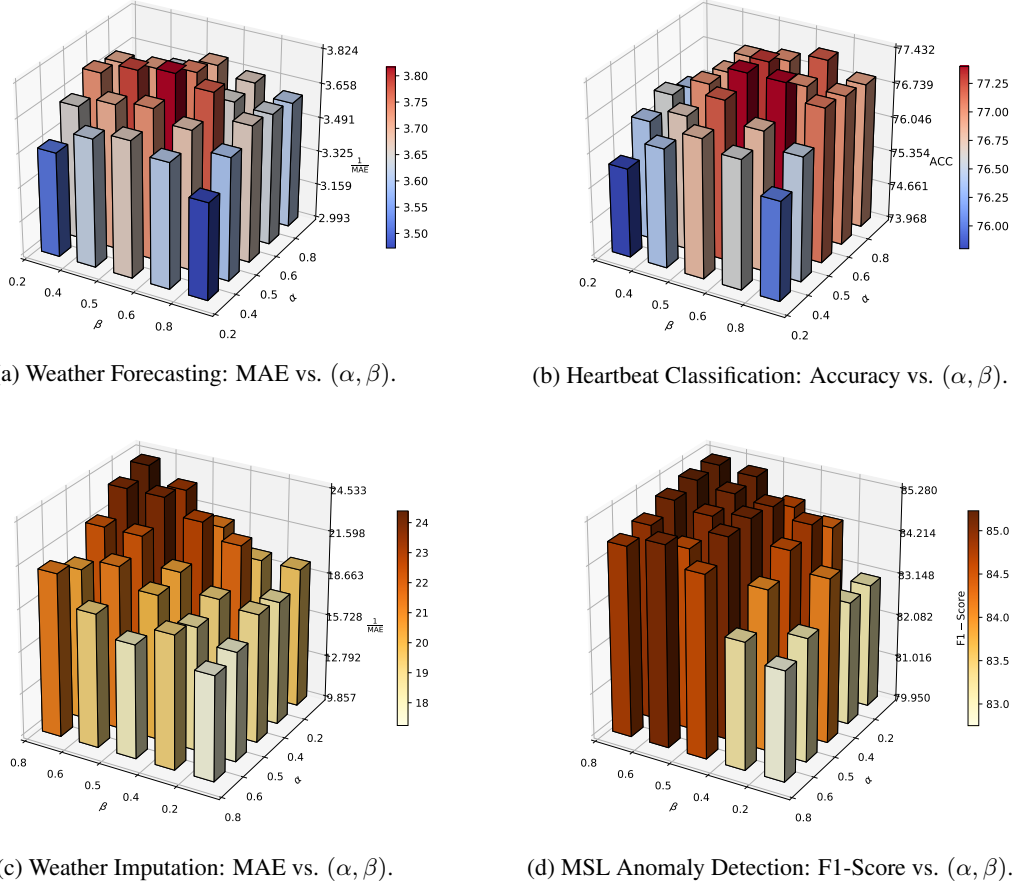


Figure 6: Sensitivity of Fusion Weights α and β Across Tasks.

Across all tasks, DeMa is most reliable when both paths remain active (i.e., neither α nor β is overly small), confirming that temporal modeling and cross-variate interaction are complementary rather than substitutable. Forecasting is relatively less sensitive to α and β (Figure 6(a)), showing only mild variation across the grid. An explanation is that long-horizon prediction is often dominated by stable structures such as trend and seasonality; thus, once the temporal path is sufficiently emphasized, the model can still perform well even under moderate fusion bias, and the variate path provides a relatively smaller marginal gain unless the dataset is strongly coupled. Similarly, classification remains stable across a wide range of (α, β) (Figure 6(b)). This is because classification primarily relies on global semantic discrimination: the stacked DuoMNet blocks can progressively aggregate high-level evidence and compensate for moderate fusion imbalance, as long as neither path is completely suppressed and both temporal and cross-variate cues are retained.

In contrast, imputation is more sensitive to the fusion weights (Figure 6(c)), because recovering missing points typically requires both local temporal continuity (temporal path) and cross-variate complementarity (variate path). Over-weighting either path can lead to incomplete recovery, e.g., temporal-only fusion may miss informative cross-variate cues, while variate-only fusion may fail to preserve fine-grained local dynamics, especially under higher missing ratios. Similarly, anomaly detection exhibits strong sensitivity (Figure 6(d)), since anomalies are rare, local patterns that demand temporal modeling to capture abrupt deviations, while cross-variate modeling helps validate abnormality via multi-sensor consistency; improper weighting may either dilute anomalies under dominant normal patterns or amplify spurious fluctuations, increasing false alarms. These observations suggest that α and β should be selected in a task-aware manner, with balanced fusion being particularly important for fine-grained, locality-critical tasks such as imputation and anomaly detection.

5 RELATED WORK

Transformer-based Time Series Models. Transformers have become a dominant paradigm for multivariate time series (MTS) modeling due to their strong capability of capturing pairwise dependencies with a global receptive field. Representative approaches include Informer [20], Fedformer [21], Autoformer [22], Pyraformer [23], PatchTST [8], Crossformer [24], and UniTime [63]. A fundamental limitation of these models lies in the quadratic complexity of self-attention with respect to the token length L , which hinders scalability to long-horizon settings. To alleviate this issue, sparse or structured attention has been explored to reduce the computational burden (e.g., to $\mathcal{O}(L \log L)$) [64, 20, 65], yet it may overlook informative dependencies when only a subset of interactions is retained. More recently, iTransformer [11] reformulates MTS tokens by treating each variate as a token and applying attention over variates, shifting the quadratic term from L to the number of variates N . While efficient when $N \ll L$, this design may sacrifice fine-grained local temporal interactions that are crucial for locality-sensitive tasks.

MLP-based Time Series Models. MLP-style architectures provide an attractive alternative for efficient time series modeling by replacing attention with lightweight mixing operations. Classic representatives include DLinear [18] and its variants such as RLinear [60], which adopt decomposition-aware linear mappings strategies to achieve strong forecasting performance with low computational cost. TimeMixer [19] further enhances expressiveness via MLP-based mixing across temporal and channel dimensions. Despite their efficiency, purely MLP-based designs often rely on relatively limited inductive biases for explicitly modeling complex cross-variate interactions and fine-grained dependency structures, which can restrict their generality across diverse MTS tasks beyond forecasting.

TCN-based Time Series Models. Temporal convolutional networks (TCNs) model temporal dependencies via convolutional receptive fields and have been widely used in time series forecasting and representation learning. ModernTCN [17] strengthens classical TCNs with modern architectural practices to improve both accuracy and efficiency, while TimesNet [12] leverages convolutional modeling together with period-aware representations to capture multi-period temporal patterns. Although convolution provides strong locality and parallelism, TCN-based models typically require carefully designed receptive fields to cover long-range dependencies, and explicit cross-variate interaction modeling is still non-trivial when scaling to high-dimensional MTS.

Mamba-based Time Series Models. State space models (SSMs), particularly Mamba-style selective SSMs, have recently emerged as a compelling linear-time alternative to Transformers, demonstrating strong performance across diverse domains [28]. This progress has spurred increasing interest in adapting Mamba to time series analysis [66, 57, 67, 68, 56, 59]. For example, CMamba [66] augments Mamba-style temporal modeling with extra modules to capture cross-variate interactions, while S-Mamba [57], MambaMixer [67], MambaTS [68], and more recent variants such as Affirm [56] and SAMBA [59] explore architectural adaptations to improve effectiveness on time series benchmarks. Despite these advances, existing Mamba-based designs still face notable challenges for general MTS analysis. First, dependency entanglement is common: temporal dynamics and cross-variate interactions frequently overlap and are mixed, which can obscure task-relevant cues. Second, fine-grained cross-variate modeling remains insufficient: many methods primarily emphasize global interactions and may under-exploit local, delay-sensitive cross-variate effects. Motivated by these gaps, we propose **DeMa**, which disentangles cross-time and cross-variate dependency encoding via a dual-path design, enabling efficient yet effective modeling for general time series analysis.

6 Conclusion

In this work, we proposed DeMa, a dual-path delay-aware Mamba backbone for efficient multivariate time series analysis. DeMa explicitly decomposes the time-series context into *Cross-Time* and *Cross-Variate* components via an Adaptive Fourier Filter. These components are processed by stacked DuoMNet blocks with two parallel, scan-coupled pathways: (i) a temporal path that applies Cross-Time Scan and Mamba-SSD to capture long-range intra-series dependencies in a series-independent and parallel manner, and (ii) a variate path that applies Cross-Variate Scan and Mamba-DALA to model delay-aware inter-series interactions using DALA with both global correlation delays and token-level relative delays. The resulting representations are fused through a lightweight weighted fusion layer and projected to task-specific outputs. Extensive experiments across five mainstream tasks demonstrate that DeMa achieves consistently strong accuracy while substantially reducing

training time and GPU memory usage, suggesting a favorable accuracy-efficiency trade-off and practical scalability for long-horizon and large-scale MTS modeling.

Acknowledgments

The research described in this paper has been partially supported by the National Natural Science Foundation of China (project no. 62433016 and 62537001), General Research Funds from the Hong Kong Research Grants Council (project no. PolyU 15207322, 15200023, 15206024, and 15224524), internal research funds from Hong Kong Polytechnic University (project no. P0042693, P0048625, and P0051361). This work was supported by computational resources provided by The Centre for Large AI Models (CLAIM) of The Hong Kong Polytechnic University.

References

- [1] Xiangjie Kong, Zhenghao Chen, Weiyao Liu, Kaili Ning, Lechao Zhang, Syauqie Muhammad Marier, Yichen Liu, Yuhao Chen, and Feng Xia. Deep learning for time series forecasting: a survey. *International Journal of Machine Learning and Cybernetics*, pages 1–34, 2025.
- [2] Guangyu Huo, Yong Zhang, Boyue Wang, Junbin Gao, Yongli Hu, and Baocai Yin. Hierarchical spatio-temporal graph convolutional networks and transformer network for traffic flow forecasting. *IEEE Transactions on Intelligent Transportation Systems*, 24(4):3855–3867, 2023.
- [3] Rui An, Yifeng Zhang, Ziran Liang, Wenqi Fan, Yuxuan Liang, Xuequn Shang, and Qing Li. Damba-st: Domain-adaptive mamba for efficient urban spatio-temporal prediction. *arXiv preprint arXiv:2506.18939*, 2025.
- [4] Feiyi Chen, Zhen Qin, Mengchu Zhou, Yingying Zhang, Shuiguang Deng, Lunting Fan, Guansong Pang, and Qingsong Wen. Lara: A light and anti-overfitting retraining approach for unsupervised time series anomaly detection. In *Proceedings of the ACM on Web Conference 2024*, pages 4138–4149, 2024.
- [5] Ane Blázquez-García, Angel Conde, Usue Mori, and Jose A Lozano. A review on outlier/anomaly detection in time series data. *ACM computing surveys (CSUR)*, 54(3):1–33, 2021.
- [6] Zhen Qin, Yibo Zhang, Shuyu Meng, Zhiguang Qin, and Kim-Kwang Raymond Choo. Imaging and fusing time series for wearable sensor-based human activity recognition. *Information Fusion*, 53:80–87, 2020.
- [7] A Vaswani. Attention is all you need. *Advances in Neural Information Processing Systems*, 2017.
- [8] Yuqi Nie, Nam H Nguyen, Phanwadee Sinthong, and Jayant Kalagnanam. A time series is worth 64 words: Long-term forecasting with transformers. In *The Eleventh International Conference on Learning Representations*, 2023.
- [9] Yong Liu, Haoran Zhang, Chenyu Li, Xiangdong Huang, Jianmin Wang, and Mingsheng Long. Timer: Generative pre-trained transformers are large time series models. In *Forty-first International Conference on Machine Learning*, 2024.
- [10] Gerald Woo, Chenghao Liu, Akshat Kumar, Caiming Xiong, Silvio Savarese, and Doyen Sahoo. Unified training of universal time series forecasting transformers. In *Forty-first International Conference on Machine Learning*, 2024.
- [11] Yong Liu, Tengge Hu, Haoran Zhang, Haixu Wu, Shiyu Wang, Lintao Ma, and Mingsheng Long. itransformer: Inverted transformers are effective for time series forecasting. In *The Twelfth International Conference on Learning Representations*, 2024.
- [12] Haixu Wu, Tengge Hu, Yong Liu, Hang Zhou, Jianmin Wang, and Mingsheng Long. Timesnet: Temporal 2d-variation modeling for general time series analysis. In *The Eleventh International Conference on Learning Representations*, 2023.
- [13] Ziran Liang, Rui An, Wenqi Fan, Yanghui Rao, and Yuxuan Liang. itfkan: Interpretable time series forecasting with kolmogorov-arnold network. *arXiv preprint arXiv:2504.16432*, 2025.
- [14] Hansika Hewamalage, Christoph Bergmeir, and Kasun Bandara. Recurrent neural networks for time series forecasting: Current status and future directions. *International Journal of Forecasting*, 37(1):388–427, 2021.

[15] Michael Hüskens and Peter Stagge. Recurrent neural networks for time series classification. *Neurocomputing*, 50:223–235, 2003.

[16] Minhao Liu, Ailing Zeng, Muxi Chen, Zhijian Xu, Qiuxia Lai, Lingna Ma, and Qiang Xu. Scinet: Time series modeling and forecasting with sample convolution and interaction. *Advances in Neural Information Processing Systems*, 35:5816–5828, 2022.

[17] Donghao Luo and Xue Wang. Moderntcn: A modern pure convolution structure for general time series analysis. In *ICLR*, 2024.

[18] Ailing Zeng, Muxi Chen, Lei Zhang, and Qiang Xu. Are transformers effective for time series forecasting? In *Proceedings of the AAAI conference on artificial intelligence*, volume 37, pages 11121–11128, 2023.

[19] Shiyu Wang, Haixu Wu, Xiaoming Shi, Tengge Hu, Huakun Luo, Lintao Ma, James Y Zhang, and JUN ZHOU. Timemixer: Decomposable multiscale mixing for time series forecasting. In *International Conference on Learning Representations (ICLR)*, 2024.

[20] Haoyi Zhou, Shanghang Zhang, Jieqi Peng, Shuai Zhang, Jianxin Li, Hui Xiong, and Wancai Zhang. Informer: Beyond efficient transformer for long sequence time-series forecasting. In *Proceedings of the AAAI conference on artificial intelligence*, volume 35, pages 11106–11115, 2021.

[21] Tian Zhou, Ziqing Ma, Qingsong Wen, Xue Wang, Liang Sun, and Rong Jin. Fedformer: Frequency enhanced decomposed transformer for long-term series forecasting. In *International conference on machine learning*, pages 27268–27286. PMLR, 2022.

[22] Haixu Wu, Jiehui Xu, Jianmin Wang, and Mingsheng Long. Autoformer: Decomposition transformers with auto-correlation for long-term series forecasting. *Advances in neural information processing systems*, 34:22419–22430, 2021.

[23] Shizhan Liu, Hang Yu, Cong Liao, Jianguo Li, Weiyao Lin, Alex X Liu, and Schahram Dustdar. Pyraformer: Low-complexity pyramidal attention for long-range time series modeling and forecasting. In *International conference on learning representations*, 2021.

[24] Yunhao Zhang and Junchi Yan. Crossformer: Transformer utilizing cross-dimension dependency for multivariate time series forecasting. In *The eleventh international conference on learning representations*, 2023.

[25] Vijay Ekambaram, Arindam Jati, Nam Nguyen, Phanwadee Sinthong, and Jayant Kalagnanam. Tsmixer: Lightweight mlp-mixer model for multivariate time series forecasting. In *Proceedings of the 29th ACM SIGKDD Conference on Knowledge Discovery and Data Mining*, pages 459–469, 2023.

[26] Albert Gu and Tri Dao. Mamba: Linear-time sequence modeling with selective state spaces. *arXiv preprint arXiv:2312.00752*, 2023.

[27] Tri Dao and Albert Gu. Transformers are ssms: generalized models and efficient algorithms through structured state space duality. In *Proceedings of the 41st International Conference on Machine Learning*, pages 10041–10071, 2024.

[28] Haohao Qu, Liangbo Ning, Rui An, Wenqi Fan, Tyler Derr, Xin Xu, and Qing Li. A survey of mamba. *arXiv preprint arXiv:2408.01129*, 2024.

[29] Opher Lieber, Barak Lenz, Hofit Bata, Gal Cohen, Jhonathan Osin, Itay Dalmedigos, Erez Safahi, Shaked Meir, Yonatan Belinkov, Shai Shalev-Shwartz, et al. Jamba: A hybrid transformer-mamba language model. *arXiv preprint arXiv:2403.19887*, 2024.

[30] Lianghui Zhu, Bencheng Liao, Qian Zhang, Xinlong Wang, Wenyu Liu, and Xinggang Wang. Vision mamba: Efficient visual representation learning with bidirectional state space model. *arXiv preprint arXiv:2401.09417*, 2024.

[31] Yair Schiff, Chia Hsiang Kao, Aaron Gokaslan, Tri Dao, Albert Gu, and Volodymyr Kuleshov. Caduceus: Bi-directional equivariant long-range dna sequence modeling. In *International Conference on Machine Learning*, pages 43632–43648. PMLR, 2024.

[32] Haohao Qu, Yifeng Zhang, Liangbo Ning, Wenqi Fan, and Qing Li. Ssd4rec: A structured state space duality model for efficient sequential recommendation. *arXiv preprint arXiv:2409.01192*, 2024.

[33] Yuxuan Wang, Haixu Wu, Jiaxiang Dong, Yong Liu, Mingsheng Long, and Jianmin Wang. Deep time series models: A comprehensive survey and benchmark. *arXiv preprint arXiv:2407.13278*, 2024.

[34] Lifan Zhao and Yanyan Shen. Rethinking channel dependence for multivariate time series forecasting: Learning from leading indicators. In *The Twelfth International Conference on Learning Representations*, 2024.

[35] Qingqing Long, Zheng Fang, Chen Fang, Chong Chen, Pengfei Wang, and Yuanchun Zhou. Unveiling delay effects in traffic forecasting: A perspective from spatial-temporal delay differential equations. In *Proceedings of the ACM on Web Conference 2024*, pages 1035–1044, 2024.

[36] Jiawei Jiang, Chengkai Han, Wayne Xin Zhao, and Jingyuan Wang. Pdformer: Propagation delay-aware dynamic long-range transformer for traffic flow prediction. In *Proceedings of the AAAI conference on artificial intelligence*, volume 37, pages 4365–4373, 2023.

[37] Albert Gu, Tri Dao, Stefano Ermon, Atri Rudra, and Christopher Ré. Hippo: Recurrent memory with optimal polynomial projections. *Advances in neural information processing systems*, 33:1474–1487, 2020.

[38] Mark Harris, Shubhabrata Sengupta, and John D Owens. Parallel prefix sum (scan) with cuda. *GPU gems*, 3(39):851–876, 2007.

[39] Kun Yi, Qi Zhang, Wei Fan, Shoujin Wang, Pengyang Wang, Hui He, Ning An, Defu Lian, Longbing Cao, and Zhendong Niu. Frequency-domain mlps are more effective learners in time series forecasting. *Advances in Neural Information Processing Systems*, 36:76656–76679, 2023.

[40] Yong Liu, Chenyu Li, Jianmin Wang, and Mingsheng Long. Koopa: Learning non-stationary time series dynamics with koopman predictors. *Advances in neural information processing systems*, 36:12271–12290, 2023.

[41] Zhihan Yue, Yujing Wang, Juanyong Duan, Tianmeng Yang, Congrui Huang, Yunhai Tong, and Bixiong Xu. Ts2vec: Towards universal representation of time series. In *Proceedings of the AAAI conference on artificial intelligence*, volume 36, pages 8980–8987, 2022.

[42] Albert Gu, Isys Johnson, Aman Timalsina, Atri Rudra, and Christopher Ré. How to train your hippo: State space models with generalized orthogonal basis projections. *arXiv preprint arXiv:2206.12037*, 2022.

[43] Taesung Kim, Jinhee Kim, Yunwon Tae, Cheonbok Park, Jang-Ho Choi, and Jaegul Choo. Reversible instance normalization for accurate time-series forecasting against distribution shift. In *International Conference on Learning Representations*, 2021.

[44] Dongchen Han, Ziyi Wang, Zhuofan Xia, Yizeng Han, Yifan Pu, Chunjiang Ge, Jun Song, Shiji Song, Bo Zheng, and Gao Huang. Demystify mamba in vision: A linear attention perspective. *arXiv preprint arXiv:2405.16605*, 2024.

[45] Jianlin Su, Murtadha Ahmed, Yu Lu, Shengfeng Pan, Wen Bo, and Yunfeng Liu. Roformer: Enhanced transformer with rotary position embedding. *Neurocomputing*, 568:127063, 2024.

[46] Mordechai Azaria and David Hertz. Time delay estimation by generalized cross correlation methods. *IEEE Transactions on Acoustics, Speech, and Signal Processing*, 32(2):280–285, 1984.

[47] Dongchen Han, Xuran Pan, Yizeng Han, Shiji Song, and Gao Huang. Flatten transformer: Vision transformer using focused linear attention. In *Proceedings of the IEEE/CVF international conference on computer vision*, pages 5961–5971, 2023.

[48] Artur Trindade. ElectricityLoadDiagrams20112014. UCI Machine Learning Repository, 2015. DOI: <https://doi.org/10.24432/C58C86>.

[49] Guokun Lai, Wei-Cheng Chang, Yiming Yang, and Hanxiao Liu. Modeling long-and short-term temporal patterns with deep neural networks. In *The 41st international ACM SIGIR conference on research & development in information retrieval*, pages 95–104, 2018.

[50] Chao Chen, Karl Petty, Alexander Skabardonis, Pravin Varaiya, and Zhanfeng Jia. Freeway performance measurement system: mining loop detector data. *Transportation research record*, 1748(1):96–102, 2001.

[51] Ya Su, Youjian Zhao, Chenhao Niu, Rong Liu, Wei Sun, and Dan Pei. Robust anomaly detection for multivariate time series through stochastic recurrent neural network. In *Proceedings of the 25th ACM SIGKDD international conference on knowledge discovery & data mining*, pages 2828–2837, 2019.

[52] Kyle Hundman, Valentino Constantinou, Christopher Laporte, Ian Colwell, and Tom Soderstrom. Detecting spacecraft anomalies using lstms and nonparametric dynamic thresholding. In *Proceedings of the 24th ACM SIGKDD international conference on knowledge discovery & data mining*, pages 387–395, 2018.

[53] Aditya P Mathur and Nils Ole Tippenhauer. Swat: A water treatment testbed for research and training on ics security. In *CySWater*, 2016.

[54] Ahmed Abdulaal, Zhuanghua Liu, and Tomer Lancewicki. Practical approach to asynchronous multivariate time series anomaly detection and localization. *KDD*, 2021.

[55] Anthony J. Bagnall, Hoang Anh Dau, Jason Lines, Michael Flynn, James Large, Aaron George Bostrom, Paul Southam, and Eamonn J. Keogh. The uea multivariate time series classification archive, 2018. *arXiv preprint arXiv:1811.00075*, 2018.

[56] Yuhan Wu, Xiyu Meng, Huajin Hu, Junru Zhang, Yabo Dong, and Dongming Lu. Affirm: Interactive mamba with adaptive fourier filters for long-term time series forecasting. In *Proceedings of the AAAI Conference on Artificial Intelligence*, volume 39, pages 21599–21607, 2025.

[57] Zihan Wang, Fanheng Kong, Shi Feng, Ming Wang, Xiaocui Yang, Han Zhao, Daling Wang, and Yifei Zhang. Is mamba effective for time series forecasting? *Neurocomputing*, 619:129178, 2025.

[58] Chaolv Zeng, Zhanyu Liu, Guanjie Zheng, and Linghe Kong. Cmamba: Channel correlation enhanced state space models for multivariate time series forecasting. *arXiv preprint arXiv:2406.05316*, 2024.

[59] Zixuan Weng, Jindong Han, Wenzhao Jiang, and Hao Liu. Simplified mamba with disentangled dependency encoding for long-term time series forecasting. *arXiv preprint arXiv:2408.12068*, 2024.

[60] Zhe Li, Shiyi Qi, Yiduo Li, and Zenglin Xu. Revisiting long-term time series forecasting: An investigation on linear mapping. *arXiv preprint arXiv:2305.10721*, 2023.

[61] P Kingma Diederik. Adam: A method for stochastic optimization. (*No Title*), 2014.

[62] Anthony Bagnall, Hoang Anh Dau, Jason Lines, Michael Flynn, James Large, Aaron Bostrom, Paul Southam, and Eamonn Keogh. The uea multivariate time series classification archive, 2018. *arXiv preprint arXiv:1811.00075*, 2018.

[63] Xu Liu, Junfeng Hu, Yuan Li, Shizhe Diao, Yuxuan Liang, Bryan Hooi, and Roger Zimmermann. Unitime: A language-empowered unified model for cross-domain time series forecasting. In *Proceedings of the ACM on Web Conference 2024*, pages 4095–4106, 2024.

[64] Nikita Kitaev, Lukasz Kaiser, and Anselm Levskaya. Reformer: The efficient transformer. In *International Conference on Learning Representations*, 2019.

[65] Shiyang Li, Xiaoyong Jin, Yao Xuan, Xiyou Zhou, Wenhui Chen, Yu-Xiang Wang, and Xifeng Yan. Enhancing the locality and breaking the memory bottleneck of transformer on time series forecasting. *Advances in neural information processing systems*, 32, 2019.

[66] Chaolv Zeng, Zhanyu Liu, Guanjie Zheng, and Linghe Kong. C-mamba: Channel correlation enhanced state space models for multivariate time series forecasting. *arXiv preprint arXiv:2406.05316*, 2024.

[67] Ali Behrouz, Michele Santacatterina, and Ramin Zabih. Mambamixer: Efficient selective state space models with dual token and channel selection. *arXiv preprint arXiv:2403.19888*, 2024.

[68] Xiuding Cai, Yaoyao Zhu, Xueyao Wang, and Yu Yao. Mambats: Improved selective state space models for long-term time series forecasting. *arXiv preprint arXiv:2405.16440*, 2024.